

This work was written as part of one of the author's official duties as an Employee of the United States Government and is therefore a work of the United States Government. In accordance with 17 U.S.C. 105, no copyright protection is available for such works under U.S. Law.

Public Domain Mark 1.0

<https://creativecommons.org/publicdomain/mark/1.0/>

Access to this work was provided by the University of Maryland, Baltimore County (UMBC) ScholarWorks@UMBC digital repository on the Maryland Shared Open Access (MD-SOAR) platform.

**Please provide feedback**

Please support the ScholarWorks@UMBC repository by emailing [scholarworks-group@umbc.edu](mailto:scholarworks-group@umbc.edu) and telling us what having access to this work means to you and why it's important to you. Thank you.



Contents lists available at ScienceDirect

# Atmospheric Environment

journal homepage: <http://www.elsevier.com/locate/atmosenv>

## Influence of cloud, fog, and high relative humidity during pollution transport events in South Korea: Aerosol properties and PM<sub>2.5</sub> variability

T.F. Eck<sup>a,b,\*</sup>, B.N. Holben<sup>a</sup>, J. Kim<sup>c</sup>, A.J. Beyersdorf<sup>d</sup>, M. Choi<sup>c,e</sup>, S. Lee<sup>c</sup>, J.-H. Koo<sup>c</sup>, D. M. Giles<sup>a,f</sup>, J.S. Schafer<sup>a,f</sup>, A. Sinyuk<sup>a,f</sup>, D.A. Peterson<sup>g</sup>, J.S. Reid<sup>g</sup>, A. Arola<sup>h</sup>, I. Slutsker<sup>a,f</sup>, A. Smirnov<sup>a,f</sup>, M. Sorokin<sup>a,f</sup>, J. Kraft<sup>a,i</sup>, J.H. Crawford<sup>j</sup>, B.E. Anderson<sup>j</sup>, K.L. Thornhill<sup>j</sup>, Glenn Diskin<sup>j</sup>, Sang-Woo Kim<sup>k</sup>, Soojin Park<sup>k</sup>

<sup>a</sup> NASA Goddard Space Flight Center, Greenbelt, MD, USA

<sup>b</sup> Universities Space Research Association, Columbia, MD, USA

<sup>c</sup> Yonsei University, Seoul, South Korea

<sup>d</sup> California State University, San Bernardino, CA, USA

<sup>e</sup> NASA Jet Propulsion Lab, Pasadena, CA, USA

<sup>f</sup> SSAI, Lanham, MD, USA

<sup>g</sup> Naval Research Laboratory, Monterey, CA, USA

<sup>h</sup> Finnish Meteorological Institute, Kuopio, Finland

<sup>i</sup> FiberTek Inc., Herndon, VA, USA

<sup>j</sup> NASA Langley Research Center, Hampton, VA, USA

<sup>k</sup> Seoul National University, Seoul, South Korea

### HIGHLIGHTS

- Highest AOD and PM<sub>2.5</sub> over S. Korea had significant cloud cover and/or sea fog.
- Particle volume was at least 10 times larger on high RH pollution transport days.
- Particle SSA was high (0.97–0.99 in mid-visible) on pollution transport days.
- The PM<sub>2.5</sub> was higher over central Seoul than the coast during pollution transport.

### ARTICLE INFO

#### Keywords:

Aerosol  
Air pollution  
Remote sensing  
Cloud processes  
Aerosol-cloud interaction

### ABSTRACT

This investigation examines aerosol dynamics during major fine mode aerosol transboundary pollution events in South Korea primarily during the KORUS-AQ campaign from May 1 – June 10, 2016, particularly when cloud fraction was high and/or fog was present to quantify the change in aerosol characteristics due to near-cloud or fog interaction. We analyze the new AERONET Version 3 data that have significant changes to cloud screening algorithms, allowing many more fine-mode observations in the near vicinity of clouds or fog. Case studies for detailed investigation include May 25–26, 2016 when cloud fraction was high over much of the peninsula, associated with a weak frontal passage and advection of pollution from China. These cloud-influenced Chinese transport dates also had the highest aerosol optical depth (AOD), surface PM<sub>2.5</sub> concentrations and fine mode particle sizes of the entire campaign. Another likewise cloud/high relative humidity (RH) case is June 9 and 10, 2016 when fog was present over the Yellow Sea that appears to have affected aerosol properties well downwind over the Korean peninsula. In comparison we also investigated aerosol properties on air stagnation days with very low cloud cover and relatively low RH (May 17 & 18, 2016), when local Korean emissions dominated. Aerosol volume size distributions show marked differences between the transport days (with high RH and cloud influences) and the local pollution stagnation days, with total column-integrated particle fine mode volume being an order of magnitude greater on the pollution transport dates. The PM<sub>2.5</sub> over central Seoul were significantly greater than for coastal sites on the transboundary transport days yet not on stagnation days, suggesting additional particle formation from gaseous urban emissions in cloud/fog droplets and/or in the high RH humidified

\* Corresponding author. Code 618, NASA/GSFC, Greenbelt, MD, 20771, USA.

E-mail address: [thomas.f.eck@nasa.gov](mailto:thomas.f.eck@nasa.gov) (T.F. Eck).

<https://doi.org/10.1016/j.atmosenv.2020.117530>

Received 18 December 2019; Received in revised form 23 March 2020; Accepted 17 April 2020

Available online 27 April 2020

1352-2310/© 2020 Elsevier Ltd. All rights reserved.

aerosol environment. Many days had KORUS-AQ research aircraft flights that provided observations of aerosol absorption, particle chemistry and vertical profiles of extinction. AERONET retrievals and aircraft in situ measurements both showed high single scattering albedo (weak absorption) on the cloudy or cloud influenced days, plus aircraft profile in situ measurements showed large AOD enhancements (versus dried aerosol) at ambient relative humidity (RH) on the pollution transport days, consistent with the significantly larger fine mode particle radii and weak absorption.

## 1. Introduction

Aerosol pollution is a major health and environmental issue in many areas of the world, including east-central Asia, with significant human health impacts. Epidemiological studies show that the impacts of small particles (e.g., Particulate matter with diameter less than 2.5  $\mu\text{m}$ , or  $\text{PM}_{2.5}$ ) on lungs and even subsequent absorption into the bloodstream results in a number of negative health outcomes including decreased productivity and also significantly increased mortality, from both episodic and long-term exposure (Lelieveld et al., 2015; Dominici et al., 2006; Heo et al., 2014). South Korea has been subjected to particularly high concentrations of fine mode particulate pollution over the last few decades due to rapid regional population growth and associated urban and industrial growth, but has seen gradual decreases in PM concentrations with emission controls by governments (Kim and Lee, 2018). Seoul in South Korea, currently the second largest metropolitan region on Earth, has extensive local and regional emissions of particulates and associated precursor gasses from both industrial sources and numerous vehicular sources (Guttikunda et al., 2003; Lee and Kim, 2007). In addition, under the right meteorological conditions significant transboundary transport of particulate pollution can occur, originating in China and crossing the Yellow Sea to South Korea (Choi et al., 2019a,b; Lee et al., 2019; Peterson et al., 2019). During these transboundary transport events the locally emitted pollution combines with the transported pollution resulting in particularly high levels of  $\text{PM}_{2.5}$ .

Remote sensing of total column aerosol optical depth (AOD) from satellite and ground-based instruments are often utilized to estimate the surface concentrations of  $\text{PM}_{2.5}$  and to better understand the broader regional context, with the obvious major complications of variable vertical profile of aerosol concentrations (van Donkelaar et al., 2010; Geng et al., 2015; Kim et al., 2015; Park et al., 2019) and local relative humidity (Toth et al., 2014; Reid et al., 2017; Kaku et al., 2018). However other complications in addition to vertical profile also exist in estimation of surface  $\text{PM}_{2.5}$  from measured or retrieved total column AOD in South Korea, especially in the cases of transboundary transport. One of these occurs in the context of meteorological conditions during which many transboundary transport events occur. Studies have shown that many transport events of advection of pollution from west to east across the Yellow Sea into South Korea are often associated with weak cold frontal passages (Peterson et al., 2019; Liu et al., 2013; Yoshitomi et al., 2011). Significant moisture is typically associated with these frontal systems, often including substantial cloud cover or fog that is sometimes collocated in space and time with the pollution particles and gasses. High cloud amounts are also frequently associated with the front's leading edge where high concentrations are expected (Zhang and Reid, 2009). This cloud cover makes it very difficult to utilize satellite or even ground-based remote sensing to detect the presence of the particulate pollution in many instances. For locations in China (60 km east of Beijing) and in central Seoul, Eck et al. (2018) found that a significant percentage of the highest AOD events had either few sunphotometer observations (clouds blocking the sun prevented measurements) and/or high frequency variation of short wavelength AOD associated with spatial and temporal variance of fine particles in the dynamic environments near to clouds (Eck et al., 2014). Additionally, satellite retrievals of AOD are often missed in these cloudy to partly cloudy conditions often associated with the highest AOD levels (Eck et al., 2018). Therefore regional estimates of surface  $\text{PM}_{2.5}$  in central-eastern Asia based on

remote sensing techniques that rely on satellite retrievals of AOD may inadvertently be missing some of the highest AOD events that are often associated with cloud cover and very high  $\text{PM}_{2.5}$ . Even though the surface-based network of hourly  $\text{PM}_{2.5}$  monitors is dense in South Korea resulting in robust spatial and temporal coverage of measurements even without satellite estimates (<https://www.airkorea.or.kr>), it is important to understand the relationships between aerosol concentrations and cloud cover, fog and/or RH especially in the context of evolving transboundary transport events. A related issue is that fine particles (volume radius < 1  $\mu\text{m}$ ) often swell in size when humidified and/or cloud/fog processed (Ziemba et al., 2013; Hoppel et al., 1986; Dall'Osto et al., 2009; Eck et al., 2014) thereby increasing the AOD due to the increased scattering efficiency of the swelled particles. Further, ground-based  $\text{PM}_{2.5}$  measurements have a size cutoff (2.5  $\mu\text{m}$  aerodynamic diameter; Chung et al., 2001) measured at a drier pre-specified but regionally variable relative humidity. This ambiguity, when coupled with the fact that the  $\text{PM}_{2.5}$  size cutoff includes a shoulder of coarse mode dust and sea salt further complicates the relationship between total column AOD measured at ambient RH and  $\text{PM}_{2.5}$  at the surface.

An additional aspect of the observability issue related to the potential lack of satellite detection of high AOD (especially when associated with frontal systems and associated clouds) is that the analysis of the interaction of clouds and aerosols in this region may be skewed. Comparisons of AERONET sunphotometer measured high fine mode AOD to retrievals of AOD from MODIS satellite measurements (applied to three different algorithms) for sites in east Asia by Eck et al. (2018) showed that satellite retrievals often missed many of the high AOD events, especially those associated with clouds. Additionally, cloud-aerosol interaction involving aerosol outflow from Asia and mid-latitude cyclonic weather systems in the Pacific may be significant. Both measurement and modeling studies have provided evidence which suggests that clouds are significantly affected by aerosols flowing eastward from Asia resulting in higher cloud top heights and intensified storm systems in the Pacific (Zhang et al., 2007; Wang et al., 2014).

In this paper we primarily focus on the time interval of the KORUS-AQ field campaign (Lennartson et al., 2018; Nault et al., 2018; Holben et al., 2018; Choi et al., 2019a,b) from May 1 through June 10, 2016 in South Korea and surrounding waters. We analyze sunphotometer measurements of AOD from AERONET instrumented sites plus retrievals of particle size distributions and aerosol single scattering albedo. Additionally we present analysis of in situ particle measurements of optical properties and chemical composition made from the DC-8 campaign aircraft, sometimes from altitudinal profile flights over the AERONET sites. Furthermore, we present spatially distributed time series data of operational hourly  $\text{PM}_{2.5}$  data made by the monitoring network of the South Korean National Institute of Environmental Research (NIER), to attempt an improved understanding of surface particulate matter concentrations in relation to both transboundary transport and stagnation events. However, this is not an investigation on the correlation between AOD and  $\text{PM}_{2.5}$  or on how to estimate  $\text{PM}_{2.5}$  from AOD, but rather an analysis of the observed enhancements of both parameters when associated with nearby clouds and/or fog conditions. In order to try to gain a better understanding of the large increase in monthly mean fine mode AOD from May to June in South Korea (as observed in multi-year average AERONET data) we also analyzed the AERONET and  $\text{PM}_{2.5}$  data for the entire month of June 2016 in addition to examining MODIS satellite images for cloud cover conditions and the presence or absence of fog.

## 2. Instrumentation, data and methodology

### 2.1. AERONET

AERONET utilizes the CIMEL Electronique CE-318 sun-sky radiometer for its AOD and sun-sky measurements in its global network. [Holben et al. \(1998\)](#) provides a description of instruments and their use in detail. However, a brief description is provided here. The CE-318 automatically tracks the sun to provide AOD and sky radiance for retrievals with a 1.2° full field of view. There are a number of minor instrument variations between sites, but in this study the more standard instrument configuration was used with AOD measurements at eight wavelengths (340, 380, 440, 500, 675, 870, 1020, and 1640), plus 940 nm for water vapor. Sampling rates varied by site, with some sites attempting an AOD measurement every 15 min, while most made measurements approximately every 3 min to obtain high temporal resolution data. It takes ~8 s to scan all wavelengths utilizing a motor driven filter wheel to position each filter in front of the detector, repeated three times within a minute, to provide an ensemble mean and information for cloud screening as described below. Ion assisted deposition interference filters were used with full width at half maximum bandpass of 10 nm, except for the 340 and 380 nm channels at 2 nm bandpass. The estimated uncertainty in AERONET measured AOD, due primarily to calibration uncertainty, is ~0.01–0.02 at optical air mass of one for network field instruments (with the highest errors in the UV; [Eck et al. \(1999\)](#)). This estimate is consistent with [Schmid et al. \(1999\)](#) who compared AOD values derived from 4 different solar radiometers (including an AERONET sun-sky radiometer) operating simultaneously together in field conditions and found that the AOD values from 380 to 1020 nm agreed to within 0.015 (root mean squared). More recently, [Barreto et al. \(2016\)](#) found similar results with the latest version of the Cimel. The sky radiances are calibrated versus frequently characterized integrating spheres at the NASA Goddard Space Flight Center, to an absolute accuracy of ~5% or better ([Holben et al., 1998](#)).

All analyses utilized level 2 data from the new Version 3 spectral AOD product described in detail by [Giles et al. \(2019\)](#). Most notably Version 3 updated its cloud screening algorithm, that in part continues to rely on the higher temporal frequencies of cloud optical depth versus aerosol optical depth, especially optical depth triplet variability within a 1-min scanning cycle. This triplet variability is defined as the maximum minus minimum AOD of the three values taken in a 1-min time interval for each wavelength, with all spectral channels in Version 2 being checked for triplet range. In the new Version 3 cloud screening algorithm, only the 675, 870 and 1020 nm channels are checked where the triplet range for all three wavelengths must be within 0.01 or 0.015\*AOD (whichever is greater). Since fine mode AOD decreases rapidly with increasing wavelength and coarse mode AOD and/or cloud droplet optical depth is more spectrally flat, the triplet variance at longer wavelengths is more attributable to super-micron radius particle/droplet variation (dust or cloud). A secondary cloud screening check is made using the 440–870 nm Ångström Exponent; if the value exceeds 1.0 for an instantaneous measurement then even small numbers of AOD observations per day are retained in Level 2. Previously, three cloud screened observations per day were required in Version 2 Level 2 database. Finally, there is a cloud-screening check in Version 3 for cirrus that does not utilize temporal variance for cloud detection, but rather relies on the sky radiances within six degrees scattering angle of the sun. If the angular slope in scattering angle of the measured sky radiances in the solar aureole is sufficiently steep then there likely are cirrus cloud crystals present (due to very strong forward scattering) and there is a threshold on this angular dependence for determining cirrus presence ([Giles et al., 2019](#)). This check is particularly important for the current study as Southeast Asian data has been shown to suffer from cirrus contamination ([Chew et al., 2011](#)). The complete set of Version 3 cloud screening and Quality Assurance algorithms are provided in [Giles et al. \(2019\)](#).

#### 2.1.1. AERONET inversion methodology

The almucantar sky radiance scans made by the CIMEL instruments are performed at fixed elevation angles equal to the solar elevation with  $\pm 180^\circ$  azimuthal sweeps made sequentially at four wavelengths (440, 675, 870, and 1020 nm). These are made in both the morning hours and afternoon hours at optical airmasses of 4, 3, 2, and 1.7 (75, 70, 60, 54° solar zenith angle (SZA) respectively) plus once per hour in between. AERONET retrievals are also made utilizing hybrid sky scans with the new Cimel instruments version Model-T. The sky scan made with the hybrid methodology simultaneously moves in both the azimuthal and zenith angle directions, thus performing a scan that is in general intermediate between the almucantar and principal plane (varies the zenith angle while maintaining a fixed azimuth).

Hybrid and almucantar directional scan radiance data are combined with measured AOD data at identical wavelengths to retrieve optically equivalent column-integrated volume size distributions and aerosol refractive indices utilizing the algorithms as developed by [Dubovik and King \(2000\)](#) and [Dubovik et al. \(2006\)](#). These retrieved aerosol properties are utilized to derive additional parameters such as asymmetry parameter, single scattering albedo, and phase function. Only the new Version 3 Level 2 (and when noted Level 1.5) retrievals with the quality controls described in [Holben et al. \(2006\)](#) are presented in this study (see [Sinyuk et al., 2020](#) for details). The percentage particles of spheroidal and spherical shape required to give the best fit to the measured angular distribution of spectral sky radiances is also determined by the AERONET retrieval algorithm. [Dubovik et al. \(2006\)](#) provides further details on these retrieval algorithms.

In this study, only almucantar scans taken at solar zenith angles greater than  $\sim 50^\circ$  are analyzed and presented in order to ensure sky radiance measurements over a sufficiently wide range of scattering angles. The scattering angle range of measured sky radiances for an almucantar scan performed at 50° SZA is 100° while at 75° SZA it is 150°. However, the newly developed hybrid scans available only with the recent Model-T Cimels can provide directional sky radiance measurements with 100° scattering angle range at a solar zenith angle of only 25°. Additional cloud screening for hybrid and almucantar sky radiance measurements (first the AOD must pass the level 2 quality control and cloud screening) is performed through the requirement of symmetrical sky radiances on both sides of the sun at equal scattering angles. These radiances from both sides of the scan that meet the symmetry threshold are then averaged before being used as input to the AERONET retrieval. Directional sky radiance measurements that are asymmetrical at a given scattering angle (due to inhomogeneous aerosol distributions or cloud on one side) are eliminated, and a retrieval only reaches Level 2 when the minimum number of measurements required in defined scattering angle ranges are met (see [Holben et al. \(2006\)](#)). However, the hybrid criterion for the last scattering angle bin has a different minimum scattering angle limit ( $\geq 75^\circ$ ) than almucantars ( $\geq 80^\circ$ ) and a different minimum number of symmetric scattering angles ( $N = 2$ ) than almucantars ( $N = 3$ ), due to somewhat fewer scattering angle range measurements in the hybrid scan. [Dubovik et al. \(2000\)](#) found these AERONET inversions to be stable as determined by perturbation analyses accounting for random errors, instrumental data offsets and known uncertainties in the atmospheric radiation model.

Although few direct comparisons of size distributions between AERONET retrievals and in situ measurements have yet been published, there are several specific regional aerosol types that have been compared. For example, for biomass burning aerosols [Reid et al. \(2005\)](#) compared regional mean volume median radii from source regions in southern Africa, South America, boreal zone and temperate North America and found that AERONET retrievals versus in situ measurements of the diameter of fine mode particles were often within  $\sim 0.01 \mu\text{m}$  of each other. In the Arabian Sea for fine mode pollution particles observed during the INDOEX experiment, [Clarke et al. \(2002\)](#) showed volume size distribution lognormal fits from both aircraft and ship in situ measurements where the average accumulation mode volume peak

radius values under high aerosol loading conditions ranged from 0.17  $\mu\text{m}$  to 0.18  $\mu\text{m}$  with corresponding geometric standard deviations (widths) of 1.51 (for ship) and 1.43 (for aircraft). This compares very well to AERONET retrievals made at Kaashidhoo Island in the Maldives (in the INDOEX region), for observations when  $\text{AOD}(440\text{ nm}) > 0.4$ , of median radius of 0.18  $\mu\text{m}$  and width of 1.49 (1998–2000 multi-year average Version 2 values). Recently, Schafer et al. (2019) compared time and location matched in situ measured fine mode size distributions with AERONET retrievals from aircraft profiles at three locations in the US. They found that when the in situ data were corrected for ambient RH conditions the agreement with the remote sensing retrievals was excellent, with fine mode peak radius differences averaging 0.011  $\mu\text{m}$ . For larger sub-micron size aged Pinatubo volcanic stratospheric aerosols, Eck et al. (2010) discussed the relatively close agreement between in situ observations from stratospheric aircraft of 0.53  $\mu\text{m}$  effective radius as reported by Pueschel et al. (1994) to AERONET retrievals made from observations in 1993 of  $\sim 0.56\text{ }\mu\text{m}$  peak volume radius. For coarse mode particles (with super-micron radius), Reid et al. (2006, 2008) found excellent agreement between AERONET retrieved and in situ measured size for sea salt and desert dust aerosol, respectively. For aerosols of maritime origin, Smirnov et al. (2003) showed reasonable agreement between AERONET retrievals and in situ measurements of sea salt dominated coarse mode size distributions. Additionally, for coarse mode dust size distributions in the Sahel region of West Africa Johnson and Osborne (2011) have shown good agreement between AERONET retrievals and in situ measurements from aircraft.

In this study, we followed the guidance from Dubovik et al. (2000) that only almucantar retrievals where 440 nm AOD is greater than 0.4 be used for analysis of spectral refractive indices and single scattering albedo. In southern Africa, for strongly absorbing fine mode dominated biomass burning aerosols, Leahy et al. (2007) found good agreement in 550 nm single scattering albedo, with differences between in situ measurements and AERONET retrievals of  $-0.01$ . In the mid-Atlantic region of the United States for weakly absorbing anthropogenic fine mode dominated aerosol, Schafer et al. (2014) found excellent agreement between aircraft vertical profiled in situ measurements of single scattering albedo (550 nm) and AERONET retrieved values (estimated at 550 nm from the mean of 440 and 675 nm values), with an average difference of only  $\sim 0.01$  for spatially and temporally matched observations. These offsets are significantly smaller than the nominal  $\sim 0.03$  uncertainty of AERONET SSA in these circumstances.

## 2.2. Airborne in situ measurements

Airborne optical properties were measured by the NASA Langley Aerosol Research Group (LARGE). Air was sampled with an isokinetic inlet which efficiently passes particles with diameters less than 4  $\mu\text{m}$  (McNaughton et al., 2009). An integrating nephelometer (TSI, Inc. model 3563) measured scattering coefficients at 450, 550, and 700 nm, which were corrected for truncation errors according to Anderson and Ogren (1998). One nephelometer measured scattering under dried conditions (20%) while a second nephelometer measured scattering after humidification to 80%. A single-parameter monotonic growth curve was then used to calculate the scattering at ambient RH (Gasso et al., 2000), which was determined based on water vapor concentration measured by an open-path diode laser hygrometer (Diskin et al., 2002), static temperature, and pressure.

A particle soot absorption photometer (PSAP, Radiance Research) measured absorption coefficients at 470, 532, and 660 nm, which were corrected for filter scattering according to Virkkula (2010). To align wavelengths, the measured Ångström exponent was used to adjust the scattering at 550 to 532 nm (Ziemba et al., 2013). The scattering (at ambient RH) and absorption allowed for calculation of ambient extinction (scattering + absorption) and SSA (scattering/extinction). Similarly, the dry extinction was calculated. Profiles of dry and ambient aerosol extinction over Seoul allowed for determination of dry and

ambient AOD (Beyersdorf et al., in preparation). The ratio of ambient AOD to dry AOD is referenced as AOD enhancement. High water content of aerosol results in large AOD enhancement.

Additionally, LARGE measured in situ dried aerosol size distributions by a Laser Aerosol Spectrometer (TSI Model 3340). Aerosol composition measurements were made by the NOAA Single Particle Soot Photometer (SP2) and the University of Colorado at Boulder High Resolution Time of Flight Aerosol Mass Spectrometer (HR-TOF AMS). Composition measurements during KORUS are summarized in Nault et al. (2018), Lamb et al. (2018) and Jordan et al. (2020).

## 2.3. NIER hourly $\text{PM}_{2.5}$

We performed quality control of the  $\text{PM}_{2.5}$  data prior to the analysis and site comparisons. Sites with hourly  $\text{PM}_{2.5}$  that exhibited values  $> 150\text{ }\mu\text{g}/\text{m}^3$  were excluded, also sites with constant single digit values for several hours that abruptly jumped to  $> 20\text{ }\mu\text{g}/\text{m}^3$  were also excluded. The  $150\text{ }\mu\text{g}/\text{m}^3$  values were significantly higher than occurred in the majority of sites (some sites showed values  $> 300\text{ }\mu\text{g}/\text{m}^3$ ) and the abrupt jumps in  $\text{PM}_{2.5}$  after periods of several hours of constant value were deemed to be non-physical. One site in coastal region was excluded due to a location immediately adjacent to a very densely built area (as seen from MODIS satellite images). Fig. 1 shows the locations of the  $\text{PM}_{2.5}$  sites that were analyzed in this study. Also shown are the principal AERONET sites that were analyzed.

## 3. Aerosol and clouds/fog - KORUS-AQ field campaign time period

We initially focus on the May 1 – June 10, 2016 time interval of the KORUS-AQ campaign since a multitude of data involving numerous in situ and remote sensing instruments from both ground-based and aircraft platforms were acquired. Additionally, many studies of data from KORUS-AQ have been published thereby enabling us to expand upon and build from these previous findings. The investigation of Peterson et al. (2019) has shown the dominant role that meteorology had in affecting pollution concentrations in South Korea during the KORUS-AQ campaign in 2016. In particular Peterson et al. (2019) identified several synoptic meteorological regimes that were dominant during portions of the KORUS-AQ campaign. They refer to the interval of May 17 through May 22 as the stagnation period when a dominant anticyclonic circulation resulted in low cloud cover fraction, low relative humidity and relatively light winds. Almost immediately following, the interval of May 25 through May 31 was identified as a long-range pollution transport interval characterized by weak cold frontal passages, relatively high cloud cover fraction and high relative humidity. In this section we will primarily focus on these two KORUS-AQ campaign time intervals but also discuss the relatively high particulate pollution dates that occurred during June 9–10.

The time series of the AERONET measured AOD at 675 nm and the retrieved fine mode volume median radius at the Yonsei University site (central Seoul) for the KORUS-AQ field campaign period (when the DC-8 aircraft flights occurred) is shown in Fig. 2a. The AOD data are all Level 2, however the particle radius data shown are Level 1.5 since there were some days when there were no Level 2 retrievals of aerosol size distribution, primarily due to extensive cloud cover. We did limit the sky error of all of these retrievals to the same thresholds utilized in Level 2 (from 5% to 8% dependent on AOD level; Holben et al., 2006) to ensure that these retrievals resulted in good agreement between measured and computed angular sky radiances. It is noted that the transboundary transport days (May 25–27 and May 31) when AOD and fine mode volume median radius were high also typically showed significant cloud cover and/or fog, due to the presence of weak cold frontal passages coincident with the transport days (Peterson et al., 2019). MODIS satellite images from May 25 and 26 (Fig. 3a and b) show the presence of clouds and fog in the region on these days. Fig. 2b presents a similar time

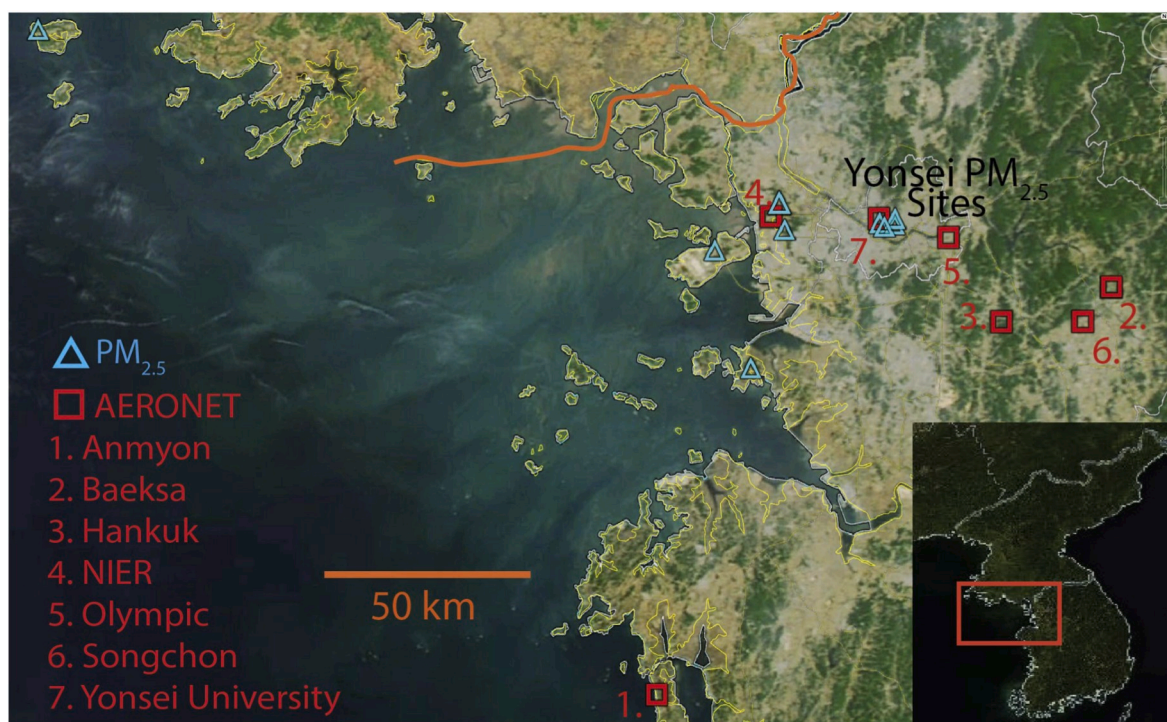


**Fig. 1.** Locations of PM<sub>2.5</sub> monitoring stations (NIER) which were utilized in this study, shown with blue markers. Four sites (easternmost on map) were within 5 km of Yonsei University in central Seoul, 4 sites (widely separated) were to the west in the coastal region (~25–50 km from Yonsei U.), and one site, Baengnyeong, was 210 km to the WNW of Yonsei University. Also shown are the principal AERONET sites that were analyzed (marked with red squares). (For interpretation of the references to colour in this figure legend, the reader is referred to the Web version of this article.)

series plot of hourly PM<sub>2.5</sub> data, which is an average of four sites within 5 km of the Yonsei University AERONET site in central Seoul plus the average of four widely separated sites located relatively close to the coast. The shaded stagnant and transport time intervals shown follow the meteorological analyses presented in Peterson et al. (2019). Note the similarity in the temporal pattern of the AOD/fine radius time series as compared to the PM<sub>2.5</sub> time series, especially for the maxima in all parameters during the transboundary transport dates within the May 25 through May 31 time interval. The AOD and fine radius also show significantly elevated values for June 9 & 10 (even though transport from China was not as dominant or direct), while the relative magnitude of the increase for PM<sub>2.5</sub> is not as high. These two days with be discussed in more detail below. However, the second highest AOD for the campaign occurred on June 7, 2016 when there was no transboundary transport, but significant cumulus cloud cover over much of Seoul. This day will also be described in detail in the next section.

The time series of AERONET retrieved fine mode particle volume median radius (Fig. 2a) shows significantly larger radius aerosol when both AOD and PM<sub>2.5</sub> levels were elevated, especially during the dates of transport events from China when fine mode aerosol dominated (fine mode fraction of AOD (FMF) ranging from ~92% to 97%). These larger fine mode radii are almost certainly due in part to hygroscopic growth at high RH. Aircraft-based in situ data from LARGE show that AOD nearly doubled from dry to moist ambient condition RH values on the transboundary transport dates (Table 1). Further detail and analyses on particle growth and associated increased water content for the transboundary transport cases is given in Beyersdorf et al. (in preparation). Additionally, significant cloud and/or fog on these days also strongly implies that aqueous phase aerosol processing likely occurred, which can be another possible mechanism for enhanced particle production in polluted conditions (Wang et al. (2016)). Cloud or fog processing of aerosols also results in very large fine mode particles, sometimes with a middle-sized mode of 0.44 μm radius in the volume distribution. AERONET volume size distribution retrievals showed fine mode aerosol

volume more than an order of magnitude larger on pollution transport dates and fog processing dates as compared to air stagnation dates (Fig. 4). Also note in Fig. 4 that the maximum fine mode radius on May 31, 2016 (a transboundary transport date) showed very large values, between 0.4 μm and 0.5 μm. Fine mode particles of this size indicate either extreme hygroscopic growth and/or cloud or fog droplet processing as strongly suggested in many other AERONET retrievals (Eck et al., 2012, 2018; Li et al., 2014) and as also observed from in situ measurements during fog (Dal'Ossto et al., 2009). From the peak radius values shown in Table 1, we compute the transport/stagnation day ratios of aerosol volume and aerosol surface area for these specific particle sizes. The aerosol volume ratio for particles at peak concentration ranges from ~6 to ~14, indicating about an order of magnitude increase on the cloudy and/or foggy transport dates compared to the stagnation days. The aerosol surface area ratios are similarly high at ~3 to ~6. These large increases in aerosol volume and surface area may have significant implications for potential reactions in particles during these transport events, including possible gas-to-particle conversions.

Both measured and retrieved aerosol properties were consistent with particles predominately in the fine mode particle size range during transport events, as single scattering albedo (SSA) was very high ranging from 0.97 to 0.99, indicating very weak absorption. Comparison of SSA from LARGE in situ measured to AERONET retrieved values for stagnation and transport and/or fog days showed very good agreement, generally to within 0.015 or less (Table 2). The much higher SSA on the pollution transport days (from both independent methods) is consistent with larger particle size from aerosol humidification and/or cloud/fog processing. These large fine mode particles have high scattering efficiency thereby resulting in higher SSA than smaller radius fine particles. Additionally, water content in the aerosol may result in lower particle absorption, since water is a non-absorbing component.

Further evidence of larger sized fine particles is that the Angstrom exponents were relatively low from both LARGE and AERONET data for these fine-mode dominated events consistent with the retrievals of large

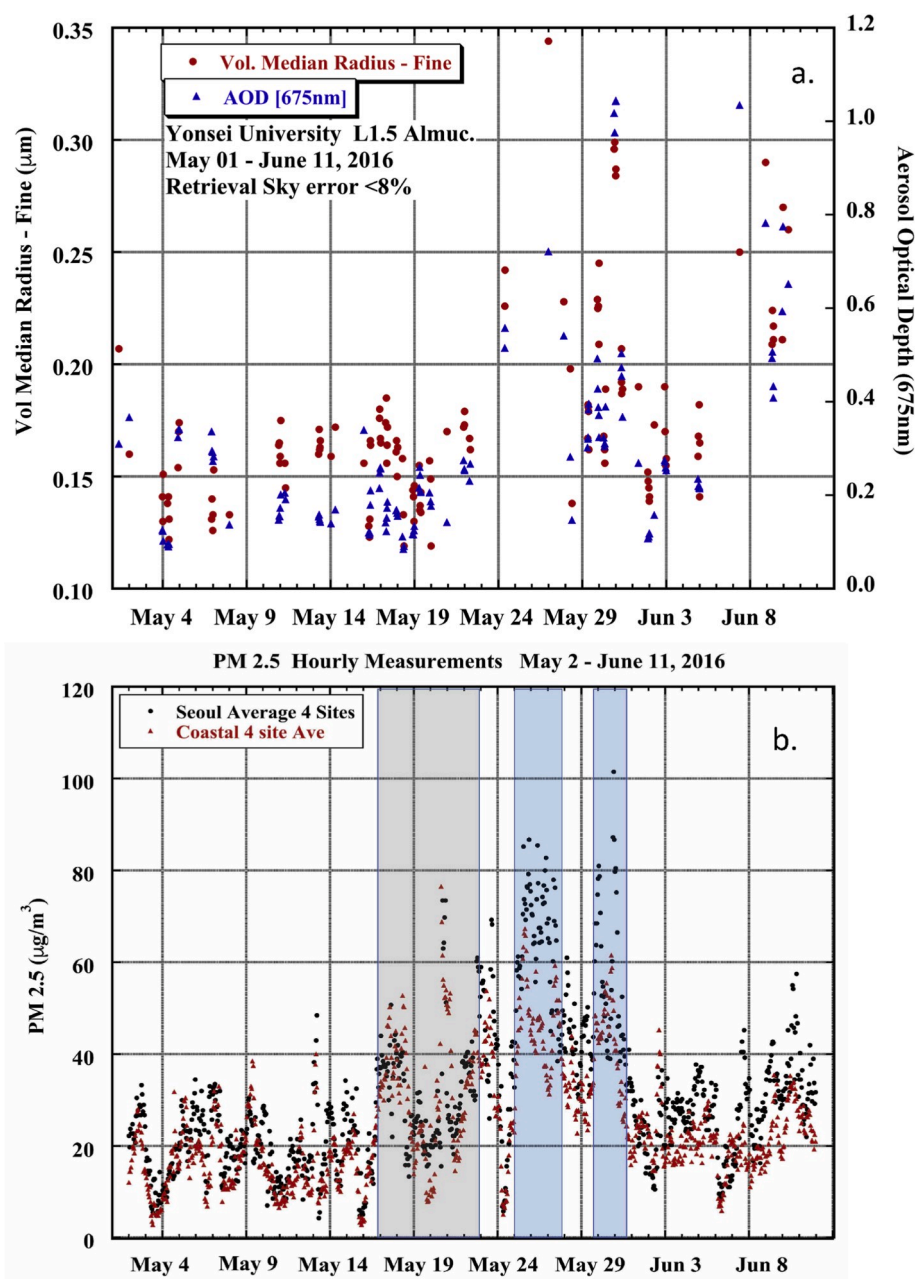


Fig. 2. (a.) Time series of the AERONET almucantar retrievals of volume median radius and measured AOD at 675 nm for the Yonsei University site in central Seoul from May 01 through June 10, 2016. (b.) Time series of hourly PM<sub>2.5</sub> for a central Seoul region (4-site average) compared with an average of 4 coastal sites. The stagnation period of May 17–23, 2016 is shaded in gray while the major transboundary transport intervals in late May are shaded in blue. (For interpretation of the references to colour in this figure legend, the reader is referred to the Web version of this article.)

fine mode particles from AERONET. The relatively strong wavelength dependence of Angstrom exponents from AERONET for these events, approximately twice as large for the 870–1020 nm wavelength interval as for 380–500 nm ( $\sim 0.5$ – $0.7$  at 380–500 nm and  $\sim 1.2$  to  $1.4$  for 870–1020 nm on the morning of May 31), can only be explained by large fine mode particles from Mie code calculations (Reid et al., 1999; Eck et al., 1999).

The dates of June 9 and 10, 2016 were not classified as primarily trans-boundary transport days during the KORUS-AQ campaign, however there was a weak cold frontal passage on June 8 that likely transported some pollution from China. Additionally, GOCI satellite images presented in Lee et al. (2019) for June 8 show a prominent east-west oriented plume of high AOD originating in eastern China (Shandong Peninsula) and extending across the Yellow Sea to a location very close to the west coast of northern South Korea, to the west of Seoul. Both June 9 and 10 show elevated AOD and PM<sub>2.5</sub> over central Seoul, in fact the PM<sub>2.5</sub> exceeded the new South Korean standard of  $35 \mu\text{g}/\text{m}^3$  on both

of these dates. Additionally, there was fog evident over the Yellow Sea to the west of Incheon on both dates from MODIS Terra images (morning overpass time). AERONET retrievals of particle size distributions from sites in greater Seoul on both dates showed either bimodal sub-micron size distributions that are typically associated with fog processed aerosols (Eck et al., 2012; Del'Osio et al., 2009) or unimodal very large fine mode size particles that also suggest cloud processing and/or extreme humidification. It is possible that pollution that had been advected over the Yellow Sea from China accumulated in this region and was subsequently transported inland to the Seoul Metropolitan Area, potentially by sea breeze circulation driven by warmer over land temperatures than over the sea. This two-stage transport process has been proposed and observed by Miao et al. (2017) to occur over Beijing from pollution that had initially accumulated over the Bohai Sea (a western gulf of the Yellow Sea) and was then transported inland by land-sea breeze circulation.

Data from the Aerodyne Aerosol Mass Spectrometer (AMS) on the

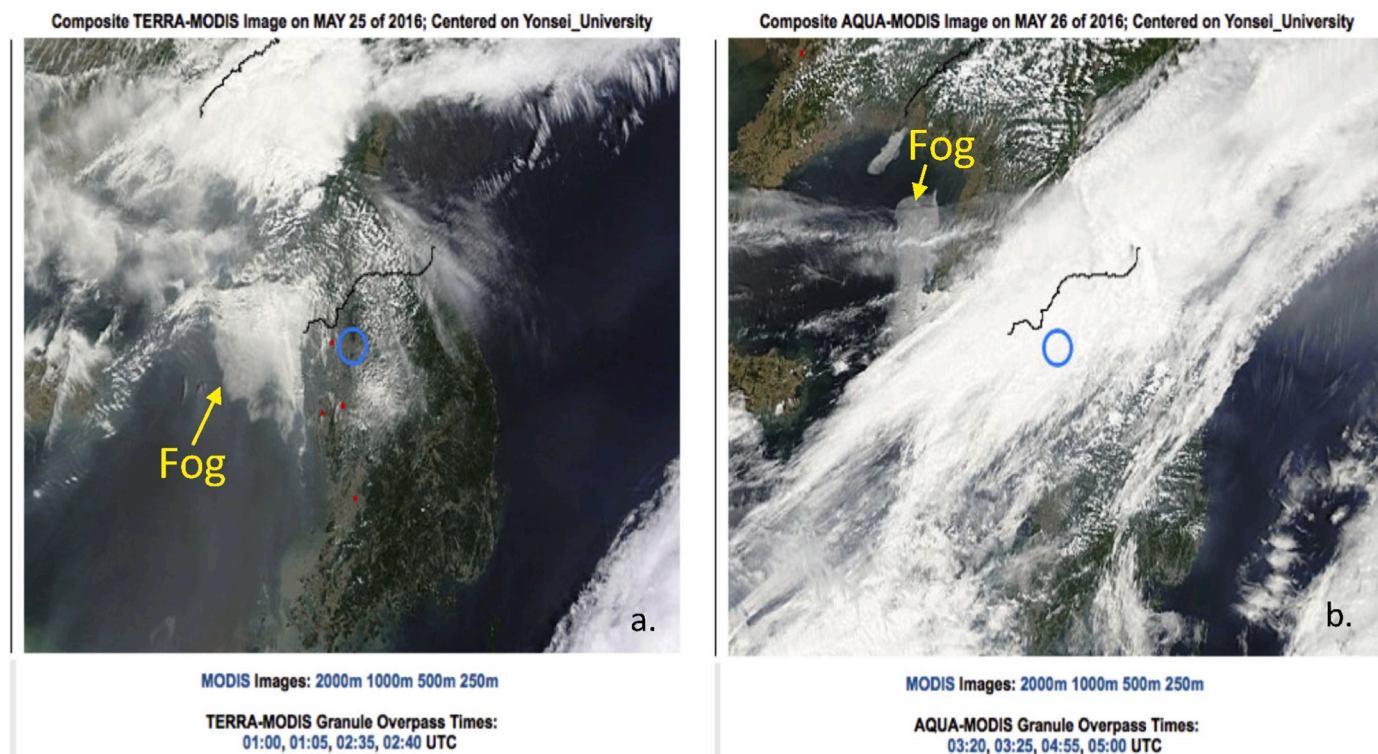


Fig. 3. a. MODIS Terra satellite image from May 25, 2016 with a blue circle centered on the Yonsei University site. b. MODIS Aqua image from May 26, 2016, also centered on the Yonsei site. Coastal fog in the Yellow Sea is noted in both images. (For interpretation of the references to colour in this figure legend, the reader is referred to the Web version of this article.)

Table 1

AERONET retrieved Fine Mode Radius and LARGE measured AOD Ambient/Dry AOD Enhancement; Primarily Morning Data; RH data from vertical profile flights; May 17 & 18 were stagnation days with little cloud and no fog; May 25,26 & 31 were transboundary transport days with clouds and/or fog; June 9 & 10 indirect influence from transport and fog.

Date in 2016	AERONET Peak Radius	LARGE AOD Amb./ Dry	RH: morning <0.5 km (0.5–1 km)	RH: mid-day <0.5 km (0.5–1 km)
May 17	0.14 $\mu\text{m}$	1.37	63% (42%)	31% (35%)
May 18	0.17 $\mu\text{m}$	1.19	41% (28%)	31% (34%)
May 25	0.33 $\mu\text{m}$ – aft.	2.01	83% (65%)	N/A
May 26	0.33 $\mu\text{m}$	1.90	N/A	57% (74%)
May 31	0.34 $\mu\text{m}$	1.67	71% (46%)	57% (57%)
June 09	0.25 $\mu\text{m}$	1.94	63% (64%)	46% (58%)
June 10	0.34 $\mu\text{m}$	1.71	74% (72%)	67% (77%)

AERONET retrievals from Songchon, Baeksa sites: ‘Taehwa spiral’ sites – Average of all available Morning retrievals except when noted (no morning retrievals on May 25); V3 Level 2 Almuantar and Hybrid retrievals except L1.5 for June 09; only one retrieval each on both May 26 and June 09.

DC-8 aircraft show that the fine mode aerosol species composition on all Chinese transport days during the KORUS-AQ campaign exhibited significant fractions of ammonia, nitrate and sulfate (inorganic particles dominated; Jordan et al., 2020) all consistent with the aerosol chemistry conducive to enhanced gas-to-particle phase reactions. High column NO<sub>2</sub> concentrations were also measured over Seoul on these days (Thompson et al., 2019). These conditions are important if the gas-to-particle formation of sulfate is occurring in the aqueous phase reactions on the fine mode particles, as NO<sub>2</sub> is a necessary oxidant (Cheng et al., 2016). The presence of ammonia is important in this fine particle reaction process as it potentially neutralizes the pH of the aerosol water thereby allowing for greater solubility of SO<sub>2</sub>. In fact, in

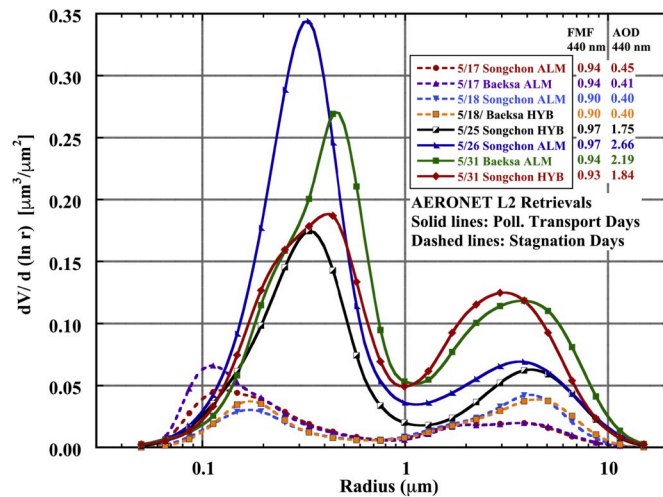


Fig. 4. AERONET size distribution retrievals show an order of magnitude greater fine mode aerosol volume on the days of pollution transport (May 25, 26, & 31) as compared to the stagnant days (May 17 & 18) with primarily local sources, low RH and no clouds. This is partly due to enhanced aerosol water on the high RH pollution transport days.

laboratory experiments Wang et al. (2016; PNAS) showed that when either NH<sub>3</sub> or NO<sub>2</sub> were absent, sulfate was not produced in the presence oxalic acid particles even at high relative humidity, while sulfate formation was strong when both NH<sub>3</sub> and NO<sub>2</sub> were present. Although sulfate production was found to be a key step in Chinese haze production (Wang et al. (2016)) due to its role in hygroscopic particle growth, other particle species are also formed at high RH, including nitrates, secondary organic aerosols, and ammonium. Kim et al. (2018) found evidence for some enhanced secondary production of sulfates and possibly nitrates

**Table 2**

Single Scattering Albedo (mid visible) Comparison – In situ LARGE (532 nm) versus AERONET retrieved; Primarily Morning Data, AERONET is 440 nm and 675 nm Average; RH data from vertical profile flights; May 17 & 18 were stagnation days with little cloud and no fog; May 25,26 & 31 were transboundary transport days with clouds and/or fog; June 9 & 10 indirect influence from transport and fog.

Date in 2016	AERONET SSA	LARGE SSA	RH: morning <0.5 km (0.5–1 km)	RH: mid-day <0.5 km (0.5–1 km)
May 17	<b>0.941</b>	<b>0.96-0.94</b>	63% (42%)	31% (35%)
May 18	<b>0.933</b>	<b>0.94-0.93</b>	41% (28%)	31% (34%)
May 25	<b>0.975 – aft.</b>	<b>0.97</b>	83% (65%)	N/A
May 26	<b>0.990</b>	<b>0.98</b>	N/A	57% (74%)
May 31	<b>0.969</b>	<b>0.97</b>	71% (46%)	57% (57%)
June 09	<b>0.993</b>	<b>1.00-0.97</b>	63% (64%)	46% (58%)
June 10	<b>0.978</b>	<b>0.97</b>	74% (72%)	67% (77%)

AERONET retrievals from Songchon, Baeksa sites: ‘Taehwa spiral’ sites – Average of all available Morning retrievals except when noted (no morning retrievals on May 25); V3 Level 2 Almicantar and Hybrid retrievals except L1.5 for June 09; only one retrieval each on both May 26 and June 09.

occurred at nighttime in the aqueous phase. RH is typically higher at night due to the absence of solar heating which results in lower temperatures. It is possible that the pH of the aerosol particles in South Korea may be too low (too acidic) to enable significant absorption of gasses to potentially enable subsequent new particle formation in aerosol water (Guo et al., 2017). However, other reactions in aerosol water may possibly occur even at lower aerosol pH levels in reactions proposed by Li et al. (2018), and this mechanism may also account for rapid production of nitrate and sulfate aerosol in pollution haze events. Moreover, other recent work by Shi et al. (2019) modeled moderate aerosol pH (~5) for haze events in China therefore suggesting that previous pathways to PM<sub>2.5</sub> production in aerosol water may be possible. In addition to reactions occurring in aerosol water, aqueous phase new particle formation in the Seoul region may have also occurred from reactions within cloud and/or fog droplets which were present during all of the major transboundary pollution events in the KORUS-AQ time interval. These droplets are much larger than aerosol particles and therefore much more likely to have higher pH than the aerosols even

after significant uptake of SO<sub>2</sub>.

The time series of the PM<sub>2.5</sub> for the Baengnyeong site (WNW of Seoul), Coastal mean and Seoul mean all show remarkably consistent temporal pattern coherence over a distance of 210 km (Fig. 5a). The correlation between the time matched hourly PM<sub>2.5</sub> data for the average of the central Seoul sites and the coastal sites average was quite high, with 60% of the variance explained. A 3-h time shift in either site resulted in reduced correlations, with ~53%–57% of the variance explained. Therefore, this suggests that there is typically minimal lag time in PM<sub>2.5</sub> between the coast and central Seoul, over a separation distance of ~25 to ~50 km. However, the correlation was much weaker between central Seoul and the Baengnyeong site (~210 km apart), with only 31% of the variance explained when the Baengnyeong data was shifted ahead by 6 h relative to the Seoul data, to account for transport time. This was the highest correlation between these sites, with 25% of the variance explained for exact time matched data (no time shift) and 25% explained for a 12-h time shift. The high correlation between central Seoul PM<sub>2.5</sub> and at the western South Korean coastal sites suggests that mesoscale to synoptic scale meteorological variation is the main driver of temporal variance in this northern South Korea region. In fact, Jordan et al. (2020) found a very high level of coherence in daily mean PM<sub>2.5</sub> for all South Korean monitoring sites on the peninsula. In particular, one meteorological aspect that may account for a significant amount of spatial coherence is sea-breeze circulations that may mix the air from over the eastern Yellow Sea with coastal and urban locations in South Korea on many days. This would particularly occur most strongly on days with low cloud cover that would intensify the solar heating of the land thereby enhancing the land-sea temperature gradient that drives the sea breeze circulation during the daytime. Likewise on cloudless nights the land surface would cool faster than the sea surface thereby setting up a possible land breeze circulation that could transport pollution towards the coast and over the sea. The sea breeze influence was strongest during the stagnant period, which was relatively dry, hot, and cloud-free. The primary transport period of 25–26 May was the opposite, with more clouds, cooler temperatures, and reduced vertical mixing. While the remainder of the transport period (27–31 May) was slightly warmer with a bit less cloud cover, it was still not as supportive of a well-defined sea breeze as the stagnation period.

The most significant PM<sub>2.5</sub> differences between central Seoul and the

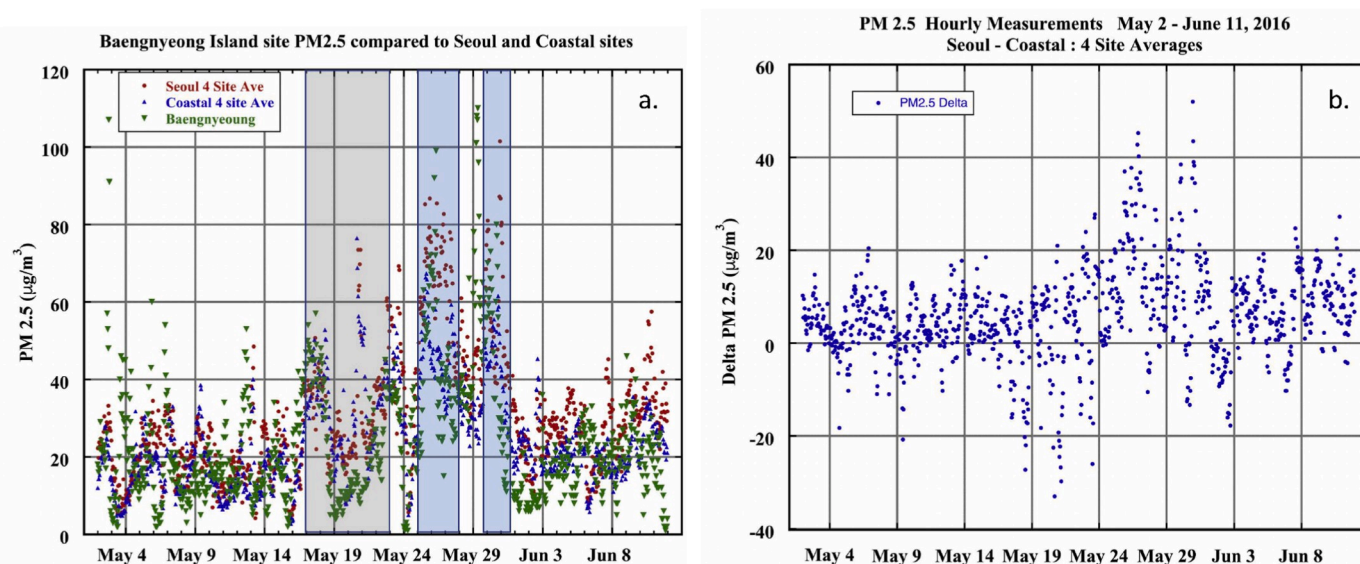


**Figure 5.** a.) Time series of hourly PM<sub>2.5</sub> measurements with the Baengnyeong site (~210 km NW of central Seoul) compared to measurements in central Seoul and the Yellow Sea coast. b.) Time series of the differences in hourly PM<sub>2.5</sub> between the central Seoul average and the coastal average. Note the higher values in Seoul versus the coastal region for the transport dates in late May. In (a.) the stagnation period of May 17–23, 2016 is shaded in gray while the major transboundary transport intervals in late May are shaded in blue.

coastal region over the time interval of the KORUS campaign occurred during major transboundary transport events that occurred during the last week of May (Fig. 5b). Comparison of  $PM_{2.5}$  data averages from 4 sites in central Seoul (within 5 km of Yonsei) to 4 sites in the Yellow Sea coastal region (west of Seoul, ~25–50 km distant) shows large differences during the China aerosol transboundary transport dates of May 25–26 with ~45% higher  $PM_{2.5}$  in Seoul (2-day mean =  $67.9 \mu\text{g}/\text{m}^3$  in Seoul;  $21.2 \mu\text{g}/\text{m}^3$  greater than the coastal mean). These  $PM_{2.5}$  differences suggest that during this major transport event perhaps 31% (calculated by  $21.2 \mu\text{g}/\text{m}^3/67.9 \mu\text{g}/\text{m}^3$ ) of the particle mass in central Seoul may have been produced over the Korean peninsula from locally emitted precursor gases. In contrast, during the six-day May 17–22 stagnation interval the differences in  $PM_{2.5}$  between the coastal sites and central Seoul sites averaged nearly zero, with values higher over the coast at times due in part to sea breeze and land breeze circulations. Note that for the Seoul versus coastal  $PM_{2.5}$  differences the aerosol transport plumes are not always homogeneous in both space and time so oscillation of the sign of the PM differences can be expected to occur. Additionally, the  $PM_{2.5}$  difference between central Seoul and Baengnyeong for May 25–26 was very similar at  $20.9 \mu\text{g}/\text{m}^3$  greater in Seoul while the difference between Seoul and Baengnyeong for the stagnation period of May 17–22 was  $\sim 9 \mu\text{g}/\text{m}^3$  (greater at Seoul), and the Coastal-Baengnyeong difference in  $PM_{2.5}$  was also  $9 \mu\text{g}/\text{m}^3$  for the stagnation period. The higher  $PM_{2.5}$  concentrations over Seoul during transboundary events suggests possible aerosol formation occurred during the Chinese pollution transport events, which also occurred simultaneously with large cloud fraction and significant fog occurrence in the Yellow Sea to the west of the Seoul metropolitan Area. The mechanism for this additional PM formation may be at least partially aqueous phase production of new particles from the gaseous emission sources in Seoul, in cloud droplets or fog droplets associated with the weak cold fronts that occurred during these particular events, and which are often associated with China pollution transport events. Studies of rapid growth of  $PM_{2.5}$  in Beijing by Zhong et al. (2017, 2018), have noted that high RH is a significant factor in rapid increases in  $PM_{2.5}$  in that region. Zhong et al. (2018) show strongly increasing measured PM1 levels as RH increased in Beijing for sulfate, nitrate, organic particles and ammonium, thereby suggesting that particle formation may possibly also occur in humidified and hygroscopic swelled aerosols. Wu et al. (2019) utilized the WRF-Chem model to estimate that aerosol water is responsible for an average of ~17% of the total near-surface  $PM_{2.5}$ , primarily through secondary aerosol formation during a winter severe haze episode on the north China Plain.

#### 4. Significant increase in monthly mean fine AOD from May to June

The monthly average fine mode AOD at the Yonsei University site in central Seoul nearly doubled from May to June. The determination of fine and coarse mode AOD were from spectral deconvolution algorithm retrievals based on total AOD spectra (O'Neill et al. 2001, 2003). This rapid increase occurred in 2016 and is also a typical occurrence in other years as is seen in the 7–8 year mean climatology (Fig. 6). In fact, the average increase in monthly mean fine mode AOD (V3 level 2) from May to June was 77%. This AOD increase is likely related to the transition from dynamic, mid-latitude springtime conditions to the summer monsoon period (Kim et al., 2007). As described by Peterson et al. (2019), the low-level boundary between the warm and moist monsoonal air mass and cooler/drier mid-latitude air masses is very distinct in late spring (referred to as “Meiyu” in China, “Baiu” in Japan, and “Changma” in Korea). As this “monsoon boundary” slowly approaches Seoul from the south, the mid-latitude storm track concurrently shifts northward, frontal boundaries generally become weaker, and progression slows. This seasonal change in meteorology becomes more evident in June, favoring occasional periods of pollution transport, similar to the event analyzed during KORUS-AQ (25–31 May). Conversely coarse mode AOD peaks in

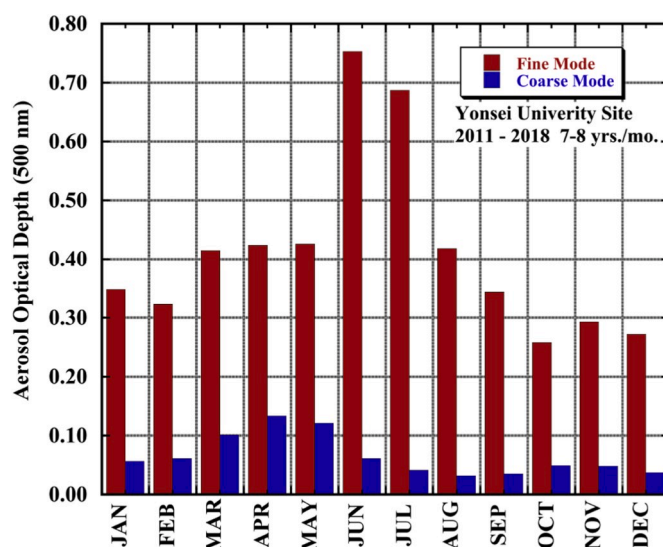


Fig. 6. Monthly means of AERONET inferred fine and coarse mode AOD (500 nm) from the Yonsei University site in central Seoul from 2011 through 2018. The SDA algorithm was utilized to separate fine and coarse mode AOD from the V3 Level 2 measured total AOD.

spring from March through May due to dynamic meteorology initiating dust transport from arid regions in mainland Asia. However even in these months the fine mode still dominates (FMF from 73% to 77%). However, monthly mean  $\text{SO}_2$  (the precursor gas to sulfate particle production) data from SCIAMACHY satellite retrievals show high concentrations of  $\text{SO}_2$  in eastern China and over the Yellow Sea for both May and June (Liu et al., 2018). Therefore the similar levels of  $\text{SO}_2$  concentrations alone between May and June do not explain the large increase in AOD between the two months, thus other mechanisms such as the concurrent meteorological changes or other particle precursors may be more important.

In order to attempt to better understand the large increase in AOD from May to June we investigated AERONET data for the entire month of June 2016, although the KORUS-AQ campaign ended on June 11, 2016. Fig. 7 shows the time series of instantaneous AOD measurements at Yonsei University for the month of June 2016. Examination of MODIS Terra and Aqua satellite images for all days when AOD at 440 nm exceeded 1.0 showed that there was either extensive fog in the Yellow Sea immediately to the west of Seoul and/or significant cloud cover over the region on every one of those high AOD dates. This is consistent with the association of cloud cover and high AOD that occurred during the last week of May 2016 when pollution was transported from China to South Korea, and also consistent with findings from previous years in this region when high AOD was often associated with cloud cover (Eck et al., 2018). This supports the previous suggestions and observations that the high AOD in association with clouds and fog is likely due to a combination of factors, including humidification of existing particles, cloud processing of particles, and possible new particle formation in these cloud and/or fog conditions. A similar large jump in monthly mean fine AOD (500 nm) from May to June also occurred in eastern China at the Xianghe AERONET site (~60 km east of Beijing) as shown in Eck et al. (2018). Therefore, this seasonal AOD shift in Seoul may be due to both regional transport of aerosol eastward and also to similar meteorological interactions involving aerosol, precursor gasses and cloud cover and/or high RH in both regions.

On June 7, which had the highest AOD during the entire month (>3.0 at 440 nm in central Seoul), there was significant dense cumulus cloud cover over the Seoul region. The MODIS images showed no clouds over the coast while inland the cumulus cloud fraction increased significantly from the Terra to the Aqua overpass times (approximately

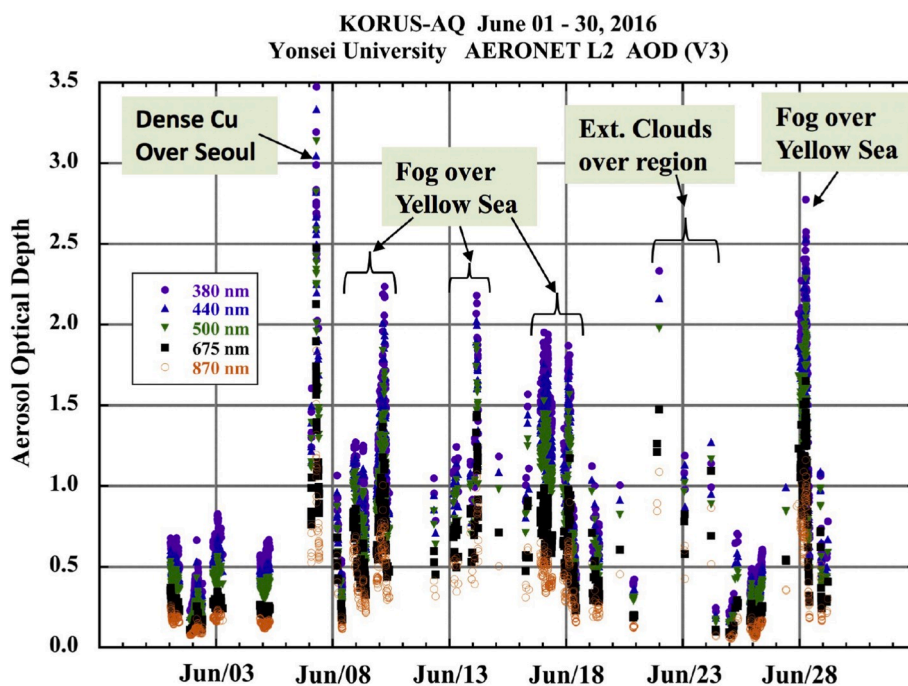
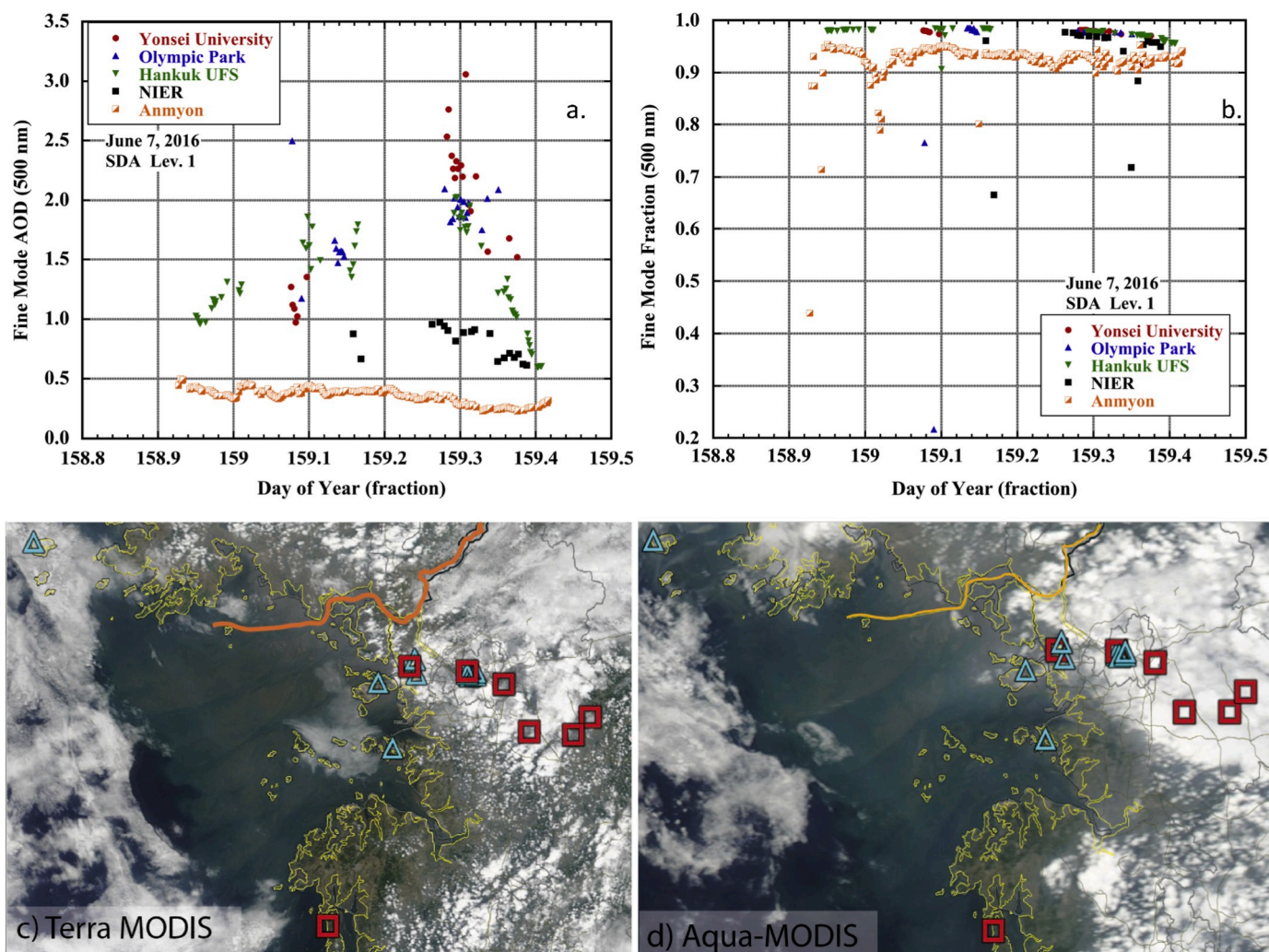


Fig. 7. Time series of AERONET measured spectral AOD at the Yonsei University site for the entire month of June 2016. The date marker indicates the beginning of each day. As noted by the brackets and arrows, all dates when AOD at 500 nm exceeded 1.0 also showed clouds in the vicinity of the site and/or fog over the Yellow Sea to the west of Seoul. (For interpretation of the references to colour in this figure legend, the reader is referred to the Web version of this article.)

1030 and 1330 local time; Fig. 8c and d.). All of the other dates during June 2016 with high AOD were more dominated by stratus type (layer clouds) or fog. This suggests that the updrafts in the cumulus clouds on June 7 may have transported aerosol vertically and that a combination of particle humidification and new particle formation in association with the clouds may have occurred. Lidar data (High Spectral Resolution Lidar; HSRL) from a site in Seoul (Seoul National University) confirm that there was some aerosol transport to altitudes of  $\sim 4$  km and higher on this date when the cumulus were present, with the cloud base height often at  $\sim 2$  km. Additionally, the AOD at 532 nm computed from cloud-free HSRL data during the partly cloudy interval were also very high, ranging from  $\sim 1.5$  to  $>4$ . It is noted in Fig. 8a that the AOD is significantly higher over Seoul than over the coastal site of Anmyon (which was cloudless) on June 07, in fact AOD was more than three to seven times higher over the urban Seoul sites of Yonsei and Olympic Park. The fine mode fractions (Fig. 8b) of this non-cloud screened data (Level 1) for all sites mainly exceeded 0.90, thereby confirming that these data are dominated by fine mode pollution aerosol with minimal cloud contamination seen in a few observations where FMF drops below 0.80. Satellite images from the geostationary GOCI sensor on June 7 in Lee et al. (2019) show relatively low AOD over the Yellow Sea ( $\sim 0.2$ – $0.4$  at 550 nm) strongly suggesting that this aerosol was not advected from China on this day. The NIER site which was located just to the west of the large cumulus cloud field had intermediate values of AOD, approximately twice as high as Anmyon, likely being influenced by the edge effect of the cumulus field. A similar large increase in AOD and in both humidification and new particle formation was observed from in situ aircraft data and surface remote sensing in association with moderate size cumulus cells over the mid-Atlantic region of the US (Eck et al., 2014). However, the aerosol size distribution retrievals (Level 2) at the Songchon, South Korea site on June 7 show very large sub-micron mode particle sizes, with the maximum volume radius  $> 0.4$   $\mu\text{m}$ , while the US mid-Atlantic case in Eck et al. (2014) which exhibited large increases in AOD with cumulus cloud development showed particle sizes that did not increase and also were relatively small with peak radius at  $\sim 0.16$   $\mu\text{m}$ . Note that there were no Level 2 almucantar or hybrid scan retrievals in

the central Seoul region on the afternoon of June 7, 2016 due to the high cloud fraction, while the Songchon site was located immediately to the southeast of this cloudy area. Therefore, it seems that the particle growth processes and/or new particle formation processes were much more vigorous in the Seoul cumulus cloud case as compared to the Maryland case, perhaps due to differences in precursor gases and their concentrations, particle properties and the size and strength of the cumulus convective cloud fields. It seems likely that high AOD associated with cumulus cloud fields over land may be in part responsible for the climatological increase in monthly mean AOD from May to June, as it was in 2016.

It is observed from daytime MODIS overpass images that fog formation in the Yellow Sea in May and June of 2016 was more prevalent in the northeast portion of the sea than in most other parts of the Sea. Dates in June 2016 that showed both high AOD and fog (from MODIS images) off of the coast west of Seoul include Jun 9, 10, 13, 14, 18, and 28. This fog formation may be due to a combination of factors, including sea surface temperatures, ocean currents and the very large tidal range of the Yellow Sea adjacent to the South Korean coast. Hu et al. (2016) computed monthly mean climatological maps of sea surface temperature (SST) for the Yellow Sea from AVHRR satellite measurements. They show a significant gradient in SST in the region to the west of the Seoul Metropolitan Area in May and June where the sea surface temperature adjacent to the land is colder and increases significantly to the west. This is consistent with the ocean currents in the Yellow Sea, where there is a cold current southward flowing adjacent to the Korean coast coupled with a warm northward flowing current farther from the coast (Naimie et al., 2001; Park et al., 2015). Therefore, it is possible that humid air that is transported in conjunction with pollution in the general westerly flow from China may reach the condensation point over these cooler near-coastal waters thereby being a potentially significant factor in fog formation over the portion of the Yellow Sea immediately to the west of Seoul. This presence of fog immediately to the west of Seoul may have some influence on the AOD and  $\text{PM}_{2.5}$  levels in Seoul when there is westerly flow, due to the extreme humidification and/or fog processing of aerosols in this fog layer which may then potentially allow for



**Fig. 8.** a. Time series of AOD (500 nm) on June 7, 2016 for five sites in S. Korea, showing higher values over central Seoul than nearer or on the coast b. Time series of the fine mode fraction of AOD, from the SDA algorithm, for the same day and sites as in 8a., indicating that these non cloud-screened AOD are dominated by fine mode particles with minimal cloud contamination. c. MODIS Terra image on morning of June 7, 2016 (at day fraction of 159.09) encompassing the sites shown in 8a. d. MODIS Aqua image on the same date, ~3 h later (at day fraction of 159.23) showing greater cumulus cloud development over the greater Seoul area.

additional particle formation in the aerosol water.

In addition to the high AOD ( $>1$  at 440 nm) in Seoul associated with clouds and/or nearby fog in June, the  $PM_{2.5}$  was also relatively high on all of these same dates, all having levels that exceeded the current Korean standard of  $35 \mu\text{g}/\text{m}^3$ . Fig. 9a shows the hourly  $PM_{2.5}$  data for the four-site central Seoul average, the four-site coastal average and the Baengnyeong site, while Fig. 9b shows the time series of the hourly differences between the Seoul and coastal sites. The  $PM_{2.5}$  values were particularly high in central Seoul on June 18, 21–23, and 28, 2016, all having some hourly values exceeding  $60 \mu\text{g}/\text{m}^3$  up to a maximum of  $100 \mu\text{g}/\text{m}^3$ . On both June 18 and 28, 2016 the MODIS images showed fog in the Yellow Sea to the west of Seoul, and on June 28 the  $PM_{2.5}$  was significantly higher in central Seoul than at the coast while on June 18 the Seoul and coastal  $PM_{2.5}$  values were relatively similar. The period of June 21–23 showed the largest differences between Seoul and coastal  $PM_{2.5}$  values with sporadically large differences (up to  $55 \mu\text{g}/\text{m}^3$ ). All three of these days had significant cloud cover, over the northern portion and sometimes over the majority of the Korean peninsula, thereby providing conditions conducive to potential aqueous phase particle production in cloud droplets. However, as noted previously, on June 7 the AOD was the highest of all days in the month, while the  $PM_{2.5}$  was far from the highest since the convection associated with the cumulus clouds over Seoul carried much of this aerosol to higher

altitudes. The convective clouds (cumulus) are initiated by strong upward motion thermals (vertical mixing) within the boundary layer, with corresponding downdrafts. The latent heating in the growing cloud then allows the air parcels to rise even higher. Regardless, the  $PM_{2.5}$  levels over central Seoul did exceed the Korean standard on this day with some hours  $>40 \mu\text{g}/\text{m}^3$ , with the values in Seoul being  $10\text{--}20 \mu\text{g}/\text{m}^3$  higher than at the coast, likely due to some vertical downdraft transport of aerosols that had formed in the clouds.

## 5. Relationships between AOD, particle size and absorption for April through June 2016

We also investigated the relationship between aerosol fine mode radius and AOD and the relationship between aerosol single scattering albedo and fine mode particle radius from the AERONET almucantar retrievals for the interval of April through June 2016 for 18 AERONET sites in South Korea. But first, a comparison of Version 3 with Version 2 almucantar retrievals (both Level 2; Fig. 10) at the Yonsei University site shows that the V3 Single Scattering Albedo (SSA) are  $\sim 0.01\text{--}\sim 0.015$  higher than in V2 (less absorption in V3), for all Angstrom Exponent intervals ranging from 0.80 (near equal mixtures of fine and coarse particles) to fine mode dominated at  $AE = 1.61$ . This is likely due in part to  $\text{NO}_2$  absorption being more completely accounted for in Version 3 sky

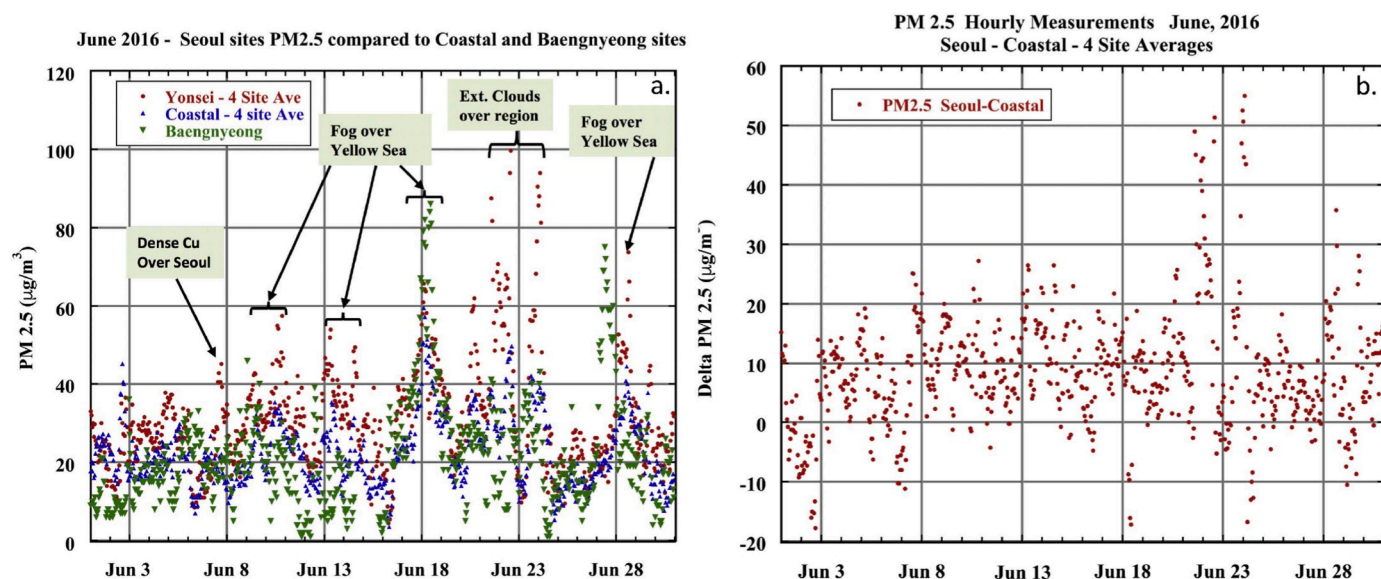


Fig. 9. Time series of hourly PM<sub>2.5</sub> measurements for Jun 01 through June 30, 2016 with the Baengnyeong site (~210 km NW of central Seoul) compared to measurements in central Seoul and the Yellow Sea coast. b.) Time series of the differences in hourly PM<sub>2.5</sub> between the central Seoul average and the coastal average. Note the much higher values in Seoul versus the coastal region for some of the days with highest PM<sub>2.5</sub> levels, especially June 22–23 and June 28. (For interpretation of the references to colour in this figure legend, the reader is referred to the Web version of this article.)

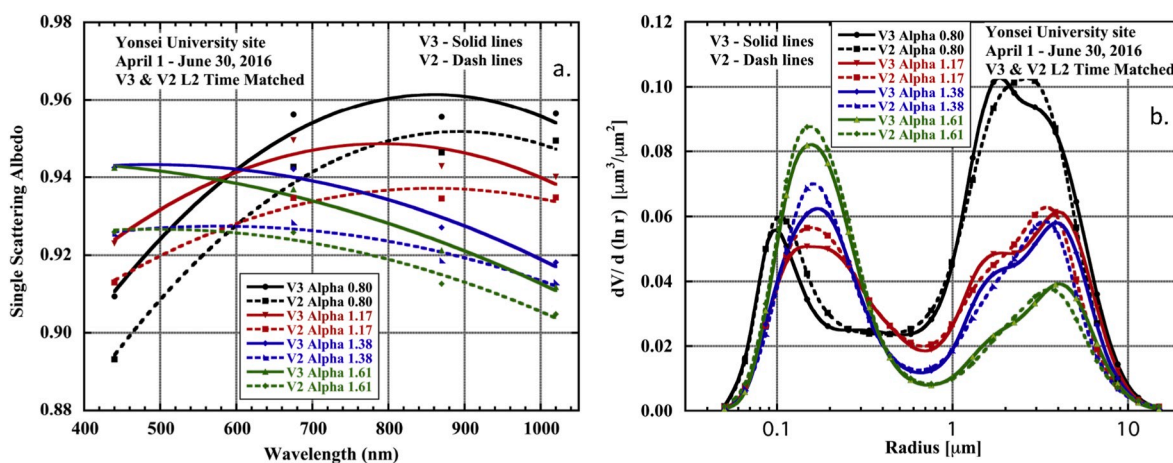


Fig. 10. a. Comparison of AERONET Version 3 to Version 2 retrievals of spectral single scattering albedo for four ranges of Angstrom Exponent (440–870 nm) ranging from 0.80 (evenly mixed fine and coarse modes) to 1.61 (fine mode dominated). These are all Level 2 retrievals at the Yonsei University site that are time matched from April 1 through June 30, 2016. Note the consistently higher values of SSA in V3 at all Angstrom Exponent levels. b.) Same as in 10a but for comparison of size distribution retrievals between V2 and V3. The size distributions are very similar for both V2 and V3 at all AE levels.

radiances, while in Version 2 the NO<sub>2</sub> absorption was partly attributed to aerosol absorption. However, the size distributions in V3 and V2 are quite similar for the entire range of Angstrom Exponents measured during this time interval.

For these 18 South Korea sites and time period, the fine mode volume median radius increased as AOD (440 nm) increased, with 44% of the variance explained by a linear fit (Fig. 11a). Particle coagulation rate increases as AOD increases (higher concentrations thereby result in larger particles), which may be a significant factor in the observed correlation. Additionally, at higher cloud cover (sometimes associated with high AOD) the RH is higher resulting in particle humidification growth, and also likely cloud processing of existing particles on some days, thus further increasing particle radius. Larger fine particles for the same number concentration results in higher AOD due to the higher scattering efficiency of the larger particles.

Fig. 11 b. and c. show that single scattering albedo increased as either AOD or fine mode radius increased due to an increase in scattering

efficiency as fine mode particle size increased and also perhaps due to particle composition changes since humidification, gas-to-particle conversion and cloud processing likely change the water content and chemical composition of the aerosol. Spectral differences in single scattering albedo can provide some useful information on the absorbing species type relative to the particle size (Derimian et al., 2008). Large values of SSA difference (440 nm minus 870 nm) at high Angstrom Exponents (fine mode dominated sizes) are associated with absorption dominated by black carbon. Decreases in spectral SSA difference as Angstrom Exponent decreased were observed (Fig. 11d) which is consistent with enhanced absorption from iron oxides in coarse mode dust (lower AE) in the blue wavelength (440 nm). However, it is also consistent with enhanced brown carbon absorption in the shorter visible wavelengths (440 nm) that may be associated with cloud processed and/or humidified aerosols that tend to have somewhat larger sized fine mode particles and therefore intermediate values of AE. For example on the morning of the transport day of May 31, 2016 at the Yonsei site the

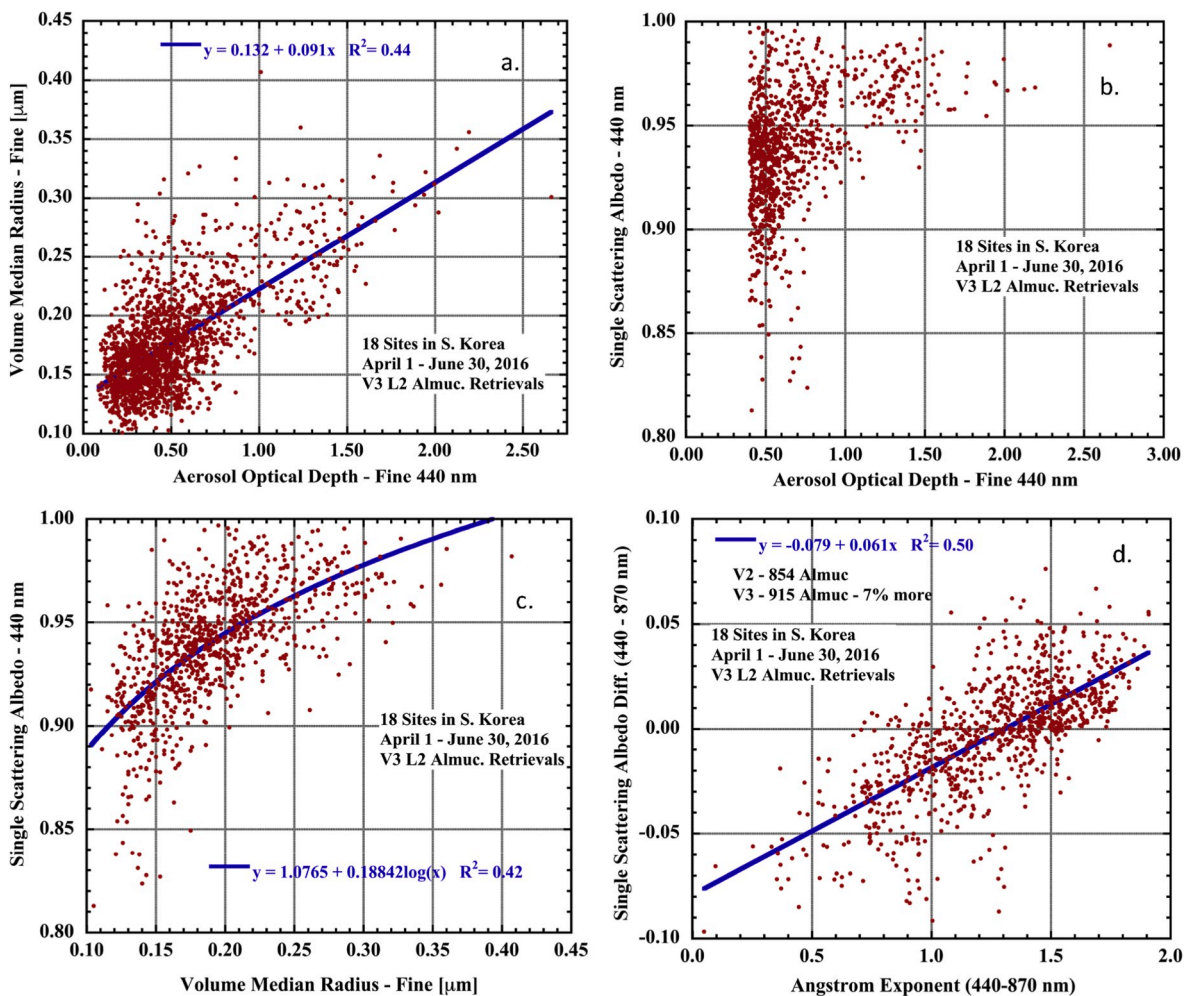


**Fig. 11.** a. Fine mode volume median radius from almucantar retrievals (V3 Level 2) versus 440 nm AOD for 18 AERONET sites in S. Korea for the three month interval of April through June, 2016. b.) Same as in Fig. 10a but for SSA at 440 nm versus AOD(440 nm). c.) SSA (440 nm) versus fine mode volume median radius for the same time interval and 18 sites. (d.) The spectral difference of SSA (440 nm) – SSA(870 nm) versus AE(440–870) for the same three month interval and 18 sites.

440–870 nm difference in SSA was 0.0 while the Angstrom exponent (440–870 nm) was  $\sim 1.0$ , and on the early morning of June 10 at the Seoul SNU site the 440–870 nm difference in SSA was  $-0.003$  while the Angstrom exponent (440–870 nm) was  $\sim 1.22$ . These highly humidified and/or cloud processed aerosol cases lie at about the midway point between the extremes in Fig. 11d. In contrast, largest positive differences in spectral SSA at the largest values of AE are consistent with black carbon as the primary absorbing species when particle size is small.

## 6. Summary and conclusions

Analyses presented in this study include AERONET remote sensing measurements and retrievals, aircraft-based in situ LARGE aerosol measurements and ground measurements of  $PM_{2.5}$  from the South Korean NIER network instruments focused on days when there was significant cloud cover over and/or fog adjacent to the coast west of Seoul. These cloudy and or foggy days (sometimes occurring during weak cold frontal passages) were often associated with direct or indirect transport of particulate pollution from eastern China. The primary interest of this study was the greater Seoul metropolitan region and the adjacent Yellow Sea region that extends  $\sim 200$  km to the west of central Seoul, with particular emphasis on, but not limited to, the KORUS-AQ field experiment study period from May 1 through June 11, 2016.

The major findings of this study are as follows:

1. Time series showed that the highest AOD and largest fine mode particle radii measured by AERONET in central Seoul during the KORUS-AQ experiment were observed to occur on the days with significant cloud cover and/or nearby fog over the Yellow Sea. Some of these dates had weak cold frontal passage and associated transboundary transport of pollution across the Yellow Sea. Measurements of AOD enhancement (the ratio of AOD at ambient RH to dried AOD) by LARGE in situ instruments indicated significant enhancements ( $\sim 1.7$ – $2$ ) on these cloudy pollution transport dates and fog dates, thereby consistent with humidification growth of particles and the large radii of the fine mode particles retrieved by AERONET.
2. Particle volume size distribution retrievals from AERONET comparing cloudy and foggy days with relatively cloudless stagnation dates show an order of magnitude greater particle volume on the cloudy and or foggy dates associated with transboundary pollution transport. The fine mode fraction of AOD at 440 nm on all of these dates ranged from 0.90 to 0.97, indicating fine mode dominance. Additionally, the size distributions on one transboundary transport date with sea fog (May 31) and two other sea fog days (June 9 and 10) showed very large bimodal submicron radii (max of  $\sim 0.4$ – $0.5$   $\mu\text{m}$  radii) that are typically associated with cloud or fog droplet processing of aerosols.
3. Retrievals of aerosol single scattering albedo from AERONET and in situ measurement of SSA from LARGE both showed very high values ( $\sim 0.97$ – $1.00$ ) on the cloudy transport dates and also dates with

nearby Yellow Sea fog. This is consistent with the large fine mode particle radii retrieved from AERONET on these days as larger particles scatter light more effectively, and as cloudy and/or fog conditions associated very high RH provide the conditions for aerosol processing in water droplets and/or particle growth from humidification. The agreement between AERONET retrievals and LARGE in situ measurements of mid-visible SSA for both cloudy high SSA dates and cloudless relatively low SSA dates was very good, within  $\sim 0.02$  or less of each other.

4. Comparison of the time series of NIER hourly PM<sub>2.5</sub> data in central Seoul with values near to the coast west of Seoul show that the largest differences in ground level PM<sub>2.5</sub> between coastal sites and central Seoul during the KORUS-AQ campaign occurred during the transboundary transport dates. This implies possible additional aerosol formation from urban region gaseous emissions in the cloud droplets on these dates and/or possible additional aerosol formation in aerosol water, although this may be highly dependent on the pH of the humidified/processed aerosol particles. The PM<sub>2.5</sub> time series during KORUS-AQ campaign period from different regions including Central Seoul, the coast west of Seoul, and Baengnyeong Island (210 km WNW of Seoul), all showed a remarkable degree of similarity in general temporal pattern. This strongly suggests that large synoptic scale meteorological processes were often a principal driver of the PM<sub>2.5</sub> dynamics in the region.
5. AERONET inferred climatological multi-year data of monthly mean AOD at the Yonsei University site in central Seoul and also for the single year 2016 both showed a large increase in fine mode AOD from May to June, with an average increase of  $\sim 75\%$  for the 8-year interval. The AERONET measured spectral AOD and surface PM<sub>2.5</sub> levels were subsequently examined for the entire month of June 2016 to better understand this large monthly jump in AOD. It was found that for June 2016 (similar to late May 2016), the highest AOD days occurred on cloudy days and/or days with fog in the Yellow Sea to the west of Seoul. Again, this implies significant humidification of aerosols in the very high RH of the cloud and near-cloud environments and also likely some cloud or fog processing of aerosol resulting in particle larger radius and increased AOD. Similarly, the highest PM<sub>2.5</sub> days in June 2016 in central Seoul also occurred during the same cloudy days or days with adjacent Yellow Sea fog, exceeding the new S. Korean standard of 35  $\mu\text{g}/\text{m}^3$  on all of these days. The largest differences in PM<sub>2.5</sub> between central Seoul versus the adjacent coastal region also occurred on some of these same days, providing further evidence that suggests additional particles are likely formed over the urban region in these cloudy and/or very humid conditions.
6. A combined analysis of retrievals from 18 AERONET sites in South Korea for the three-month period of April through June 2016 was performed in order to examine the regional relationships between fine mode radius and aerosol column concentrations and particle absorption. Increasing AOD at 440 nm was associated with increasing volume median fine mode radius with  $\sim 44\%$  of the variance explained by linear regression. This is consistent with the larger AOD values observed on the cloudy and or sea fog days when fine radius was also large, although other factors such as particle coagulation likely contribute. Single scattering albedo at 440 nm was found to increase as volume median fine mode radius increased ( $r^2 = 0.42$ , with logarithmic regression) also consistent with individual day case studies of data from both in situ LARGE data and AERONET remote sensing data during both cloudy and cloudless days. Additionally, the SSA spectral difference (440 nm–870 nm) was found to decrease with decreasing Angstrom Exponent, with linear regression explaining 50% of the variance. This decrease in SSA Difference (440–870 nm) as AE decreased is consistent with enhanced absorption from iron oxide in coarse mode dust (lowest AE values) in the blue wavelengths (440 nm), and also consistent with enhanced

brown carbon absorption, also at 440 nm, in cloud processed and/or highly humidified aerosols (intermediate AE values).

## Declaration of competing interest

The authors declare that they have no known competing financial interests or personal relationships that could have appeared to influence the work reported in this paper.

## CRediT authorship contribution statement

**T.F. Eck:** Conceptualization, Formal analysis, Investigation, Writing - original draft, Visualization. **B.N. Holben:** Project administration. **J. Kim:** Supervision, Resources. **A.J. Beyersdorf:** Validation, Formal analysis, Writing - review & editing. **M. Choi:** Investigation, Writing - review & editing. **S. Lee:** Investigation. **J.-H. Koo:** Investigation. **D.M. Giles:** Investigation, Writing - review & editing. **J.S. Schafer:** Investigation. **A. Sinyuk:** Investigation. **D.A. Peterson:** Writing - review & editing, Resources. **J.S. Reid:** Writing - review & editing, Visualization. **A. Arola:** Data curation. **I. Slutsker:** Writing - original draft, Investigation. **A. Smirnov:** Investigation. **M. Sorokin:** Investigation. **J. Kraft:** Investigation. **J.H. Crawford:** Supervision. **B.E. Anderson:** Investigation. **K.L. Thornhill:** Investigation. **Glenn Diskin:** Investigation. **Sang-Woo Kim:** Investigation. **Soojin Park:** Investigation.

## Acknowledgements

We thank Hal Maring (NASA Headquarters) and Steve Platnik (NASA GSFC) for their continuing long-term commitment and support for the AERONET project. J. S Reid's contributions were provided by the Office of Naval Research Code 322 (N0001418WX00442).

We thank the National Institute of Environmental Research (NIER) in South Korea for the hourly monitoring of PM<sub>2.5</sub> data at numerous sites in South Korea and for making these data available to KORUS-AQ researchers.

## Appendix A. Supplementary data

Supplementary data to this article can be found online at <https://doi.org/10.1016/j.atmosenv.2020.117530>.

## References

- Anderson, T.L., Ogren, J.A., 1998. Determining aerosol radiative properties using the TSI 3563 integrating nephelometer. *Aerosol. Sci. Technol.* 29 (1), 57–69. <https://doi.org/10.1080/02786829808965551>.
- Barreto, Á., Cuevas, E., Granados-Muñoz, M.-J., Alados-Arboledas, L., Romero, P., Gröbner, J., Kouremeti, N., Almansa, A.F., Stone, T., Toledano, C., Román, R., Sorokin, M., Holben, B., Canini, M., Yela, M., 2016. The new sun-sky-lunar Cimel CE318-T multiband photometer – a comprehensive performance evaluation. *Atmos. Meas. Technol.* 9, 631–654. <https://doi.org/10.5194/amt-9-631-2016>.
- Beyersdorf, A.J., Corr, C., Ortega, B., Campuzano-Jost, P., Chen, G., Diskin, G., Hite, J., Jimenez, J.L., Jordan, C.E., Nault, B.A., Nenes, A., Thornhill, K.L., Winstead, E., Anderson, B.E., 2019. Contribution of Dust & Anthropogenic Pollution to Seoul Aerosol Optical Depth in preparation.
- Cheng, Y., Zheng, G., Wei, C., Mu, Q., Zheng, B., Wang, Z., Gao, M., Zhang, Q., He, K., Carmichael, G., Pöschl, U., Su, H., 2016. Reactive nitrogen chemistry in aerosol water as a source of sulfate during haze events in China. *Sci. Adv.* 2 (12), e1601530. <https://doi.org/10.1126/sciadv.1601530>.
- Chew, B.N., Campbell, J.R., Reid, J.S., Giles, D.M., Welton, E.J., Salinas, S.V., Liew, S.C., 2011. Tropical cirrus cloud contamination in sun photometer data. *Atmos. Environ.* 45, 6724–6731. <https://doi.org/10.1016/j.atmosenv.2011.08.017>.
- Choi, J., Park, R.J., Lee, H.-M., Lee, S., Jo, D.S., Jeong, J.I., Henze, D.K., Woo, J.-H., Ban, S.-J., Lee, M.-D., Lim, C.-S., Park, M.-K., Shin, H.J., Cho, S., Peterson, D., Song, C.-K., 2019a. Impacts of local vs. trans-boundary emissions from different sectors on PM<sub>2.5</sub> exposure in South Korea during the KORUS-AQ campaign. *Atmos. Environ.* 203, 196–205. <https://doi.org/10.1016/j.atmosenv.2019.02.008>. ISSN 1352-2310.
- Choi, M., Lim, H., Kim, J., Lee, S., Eck, T.F., Holben, B.N., Garay, M.J., Hyer, E.J., Saide, P.E., Liu, H., 2019b. Validation, comparison, and integration of GOCI, AHI, MODIS, MISR, and VIIRS aerosol optical depth over East Asia during the 2016 KORUS-AQ campaign. *Atmos. Meas. Technol.* 12, 4619–4641.

- Chung, A., Chang, D.P.Y., Kleeman, M.J., Perry, K.D., Cahill, T.A., Dutcher, D., McDougall, E.M., Stroud, K., 2001. Comparison of real-time instruments used to monitor airborne particulate matter. *J. Air Waste Manag. Assoc.* 51 (1), 109–120. <https://doi.org/10.1080/10473289.2001.10464254>.
- Clarke, A.D., Howell, S., Quinn, P.K., Bates, T.S., Ogren, J.A., Andrews, E., Jefferson, A., Massling, A., Mayol Bracero, O., Maring, H., Savoie, D., Cass, G., 2002. INDOEX aerosol: a comparison and summary of chemical, microphysical, and optical properties observed from land, ship, and aircraft. *J. Geophys. Res.* 107 (D19), 8033. <https://doi.org/10.1029/2001JD000572>.
- Dall'Osto, M., Harrison, R.M., Coe, H., Williams, P., 2009. Real-time secondary aerosol formation during a fog event in London. *Atmos. Chem. Phys.* 9, 2459–2469.
- Derimian, Y., Léon, J.-F., Dubovik, O., Chiapello, I., Tanré, D., Sinyuk, A., Auriol, F., Podvin, T., Brogniez, G., Holben, B.N., 2008. Radiative properties of aerosol mixture observed during the dry season 2006 over M'Bour, Senegal (African Monsoon Multidisciplinary Analysis campaign). *J. Geophys. Res.* 113, D00C09. <https://doi.org/10.1029/2008JD009904>.
- Diskin, G.S., Podolske, J.R., William Sachse, G., Slate, T.A., 23 September 2002. Open-path airborne tunable diode laser hygrometer. In: Proc. SPIE 4817, Diode Lasers and Applications in Atmospheric Sensing. <https://doi.org/10.1117/12.453736>.
- Dominici, F., Peng, R.D., Bell, M.L., Pham, L., McDermott, A., Zeger, S.L., Samet, J.M., 2006. Fine particulate air pollution and hospital admission for cardiovascular and respiratory diseases. *JAMA J. Am. Med. Assoc.* 295 (10), 1127–1134. <https://doi.org/10.1001/jama.295.10.1127>.
- Dubovik, O., King, M.D., 2000. A flexible inversion algorithm for the retrieval of aerosol optical properties from Sun and sky radiance measurements. *J. Geophys. Res.* 105, 20,673–20,696.
- Dubovik, O., Smirnov, A., Holben, B.N., King, M.D., Kaufman, Y.J., Eck, T.F., Slutsker, I., 2000. Accuracy assessments of aerosol optical properties retrieved from AERONET Sun and sky-radiance measurements. *J. Geophys. Res.* 105, 9791–9806.
- Dubovik, O., Sinyuk, A., Lapyonok, T., Holben, B.N., Mishchenko, M., Yang, P., Eck, T.F., Volten, H., Muñoz, O., Veihelmann, B., van der Zande, W.J., Leon, J.-F., Sorokin, M., Slutsker, I., 2006. The application of spheroid models to account for aerosol particle nonsphericity in remote sensing of desert dust. *J. Geophys. Res.* 111, D11208. <https://doi.org/10.1029/2005JD006619>.
- Eck, T.F., Holben, B.N., Reid, J.S., Dubovik, O., Smirnov, A., O'Neill, N.T., Slutsker, I., Kinne, S., 1999. Wavelength dependence of the optical depth of biomass burning, urban, and desert dust aerosols. *J. Geophys. Res.* 104 (D24), 31,333–31,349.
- Eck, T.F., Holben, B.N., Sinyuk, A., Pinker, R.T., Goloub, P., Chen, H., Chatenet, B., Li, Z., Singh, R.P., Tripathi, S.N., Reid, J.S., Giles, D.M., Dubovik, O., O'Neill, N.T., Smirnov, A., Wang, P., Xia, X., 2010. Climatological aspects of the optical properties of fine/coarse mode aerosol mixtures. *J. Geophys. Res.* 115, D19205. <https://doi.org/10.1029/2010JD014002>.
- Eck, T.F., et al., 2012. Fog- and cloud-induced aerosol modification observed by the Aerosol Robotic Network (AERONET). *J. Geophys. Res.* 117, D07206. <https://doi.org/10.1029/2011JD016839>.
- Eck, T.F., Holben, B.N., Reid, J.S., Arola, A., Ferrare, R.A., Hostetler, C.A., Crumeyrolle, S.N., Berkoff, T.A., Welton, E.J., Lolli, S., Lyapustin, A., Wang, Y., Schafer, J.S., Giles, D.M., Anderson, B.E., Thornhill, K.L., Minnis, P., Pickering, K.E., Loughner, C.P., Smirnov, A., Sinyuk, A., 2014. Observations of rapid aerosol optical depth enhancements in the vicinity of polluted cumulus clouds. *Atmos. Chem. Phys.* 14, 11633–11656. <https://doi.org/10.5194/acp-14-11633-2014>.
- Eck, T.F., Holben, B.N., Reid, J.S., Xian, P., Giles, D.M., Sinyuk, A., et al., 2018. Observations of the interaction and transport of fine mode aerosols with cloud and/or fog in Northeast Asia from Aerosol Robotic Network and satellite remote sensing. *J. Geophys. Res.: Atmospheres* 123, 5560–5587. <https://doi.org/10.1029/2018JD028313>.
- Gassó, S., Hegg, D.A., Covert, D.S., Collins, D., Noone, K.J., Öström, E., Schmid, B., Russell, P.B., Livingston, J.M., Durkee, P.A., Jonsson, H., 2000. Influence of humidity on the aerosol scattering coefficient and its effect on the upwelling radiance during ACE-2. *Tellus B* 52, 546–567. <https://doi.org/10.1034/j.1600-0889.2000.00055.x>.
- Geng, G., Zhang, Q., Martin, R.V., van Donkelaar, A., Huo, H., Che, H., Lin, J., He, K., 2015. Estimating long-term PM<sub>2.5</sub> concentrations in China using satellite-based aerosol optical depth and a chemical transport model. *Rem. Sens. Environ.* 166, 262–270. <https://doi.org/10.1016/j.rse.2015.05.016>. ISSN 0034-4257.
- Giles, D.M., Sinyuk, A., Sorokin, M.G., Schafer, J.S., Smirnov, A., Slutsker, I., Eck, T.F., Holben, B.N., Lewis, J.R., Campbell, J.R., Welton, E.J., Korokin, S.V., Lyapustin, A.I., 2019. Advancements in the Aerosol Robotic Network (AERONET) Version 3 database – automated near-real-time quality control algorithm with improved cloud screening for Sun photometer aerosol optical depth (AOD) measurements. *Atmos. Meas. Technol.* 12, 169–209. <https://doi.org/10.5194/amt-12-169-2019>.
- Guo, H., Weber, R.J., Nenes, A., 2017. High levels of ammonia do not raise fine particle pH sufficiently to yield nitrogen oxide-dominated sulfate production. *Sci. Rep.* 7, Article number: 12109.
- Guttikunda, S.K., Carmichael, G.R., Calori, G., Eck, C., Woo, J.H., 2003. The contribution of megacities to regional sulfur pollution in Asia. *Atmos. Environ.* 37 (1), 11–22. [https://doi.org/10.1016/S1352-2310\(02\)00821-X](https://doi.org/10.1016/S1352-2310(02)00821-X). Article Number: PII S1352-2310(02)00821-X.
- Heo, J., Schauer, J.J., Yi, O., Paek, D., Kim, H., Yid, S.-M., 2014. Fine particle air pollution and mortality importance of specific sources and chemical species. *Epidemiology* 25 (3). <https://doi.org/10.1097/EDE.0000000000000044>. ISSN: 1044-3983/14/2503-0379.
- Holben, B.N., Eck, T.F., Slutsker, I., Tanre, D., Buis, J.P., Setzer, A., Vermote, E., Reagan, J.A., Kaufman, Y., Nakajima, T., Lavenu, F., Jankowiak, I., Smirnov, A., 1998. AERONET-A federated instrument network and data archive for aerosol characterization. *Remote Sens. Environ.* 66, 1–16.
- Holben, B.N., Eck, T.F., Slutsker, I., Smirnov, A., Sinyuk, A., Schafer, J., Giles, D., Dubovik, O., 2006. AERONET's version 2.0 quality assurance criteria, Remote Sensing of Atmosphere and Clouds. Proc. SPIE-Int. Soc. Opt. Eng. 6408, 64080Q. <https://doi.org/10.1117/12.706524>.
- Holben, B.N., Kim, J., Sano, I., Mukai, S., Eck, T.F., Giles, D.M., Schafer, J.S., Sinyuk, A., Slutsker, I., Smirnov, A., Sorokin, M., Anderson, B.E., Che, H., Choi, M., Crawford, J. H., Ferrare, R.A., Garay, M.J., Jeong, U., Kim, M., Kim, W., Knox, N., Li, Z., Lim, H.S., Liu, Y., Maring, H., Nakata, M., Pickering, K.E., Piketh, S., Redemann, J., Reid, J.S., Salinas, S., Seo, S., Tan, F., Tripathi, S.N., Toon, O.B., Xiao, Q., 2018. An overview of mesoscale aerosol processes, comparisons, and validation studies from DRAGON networks. *Atmos. Chem. Phys.* 18, 655–671. <https://doi.org/10.5194/acp-18-655-2018>.
- Hoppel, W.A., Frick, G.M., Larson, R.E., 1986. Effects on non-precipitating clouds on the aerosol size distribution in the marine boundary layer. *Geophys. Res. Lett.* 13, 125–128.
- Hu, J., Shi, M., Zhang, T., Chen, S., Wu, L., 2016. Evolution of surface cold patches in the north Yellow Sea based on satellite SST data. *J. Ocean Univ. China* 15 (6), 936–946. <https://doi.org/10.1007/s11802-016-3050-5>. ISSN: 1672-5182, 2016.
- Johnson, B.T., Osborne, S.R., 2011. Physical and validation properties of mineral dust aerosol measured by aircraft during the GERBILS campaign. *Q. J. R. Meteorol. Soc.* <https://doi.org/10.1002/qj.777>.
- Jordan, Carolyn E., Crawford, James H., Beyersdorf, Andreas J., Thomas, F. Eck, Halliday, Hannah S., Nault, Benjamin A., Lim-Seok, Chang, Rokjin, Park, Gangwoong, Lee, Hwajin, Kim, Seogju, Cho, Hye, Jung Shin, Lee, Jae Hong, Jung, Jinsang, Kim, Deug-Soo, Lee, Meehye, Lee, Taehyung, Whitehill, Andrew, Szykman, James, Schueneman, Melinda Kaye, Jost, Pedro Campuzano, Jimenez, Jose L., DiGangi, Joshua P., Diskin, Glenn S., Anderson, Bruce E., Moore, Richard H., Ziemba, Luke D., Fenn, Marta A., Hair, Johnathan W., Kuehn, Ralph E., Holz, Robert E., Chen, Gao, Travis, Katherine, Shook, Michael, Peterson, David A., Lamb, Kara D., Schwarz, Joshua P., 2020. Investigation of Factors Controlling PM<sub>2.5</sub> Variability across the South Korean Peninsula during KORUS-AQ submitted to *Elementa*.
- Kaku, K.C., Reid, J.S., Hand, J.L., Edgerton, E.S., Holben, B.N., Zhang, J., Holz, R.E., 2018. Assessing the challenges of surface-level aerosol mass estimates from remote sensing during the SEAC<sup>4</sup>RS and SEARCH campaigns: baseline surface observations and remote sensing in the southeastern United States. *J. Geophys. Res.: Atmospheres* 123, 7530–7562. <https://doi.org/10.1029/2017JD028074>.
- Kim, S.W., Yoon, S.-C., Kim, J., Kim, S.-Y., 2007. Seasonal and monthly variations of columnar aerosol optical properties over East Asia determined from multi-year MODIS, LIDAR, and AERONET sun/sky radiometer measurements. *Atmos. Environ.* 41, 1634–1651.
- Kim, P.S., Jacob, D.J., Fisher, J.A., Travis, K., Yu, K., Zhu, L., Yantosca, R.M., Sulprizio, M.P., Jimenez, J.L., Campuzano-Jost, P., Froyd, K.D., Liao, J., Hair, J.W., Fenn, M.A., Butler, C.F., Wagner, N.L., Gordon, T.D., Welti, A., Wennberg, P.O., Crouse, J.D., St Clair, J.M., Teng, A.P., Millet, D.B., Schwarz, J.P., Markovic, M.Z., Perring, A.E., 2015. Sources, seasonality, and trends of southeast US aerosol: an integrated analysis of surface, aircraft, and satellite observations with the GEOS-Chem chemical transport model. *Atmos. Chem. Phys.* 15, 10411–10433. <https://doi.org/10.5194/acp-15-10411-2015>.
- Kim, H., Zhang, Q., Heo, J., 2018. Influence of intense secondary aerosol formation and long-range transport on aerosol chemistry and properties in the Seoul Metropolitan Area during spring time: results from KORUS-AQ. *Atmos. Chem. Phys.* 18, 7149–7168. <https://doi.org/10.5194/acp-18-7149-2018>.
- Kim, Yong Pyo, Lee, Gangwoong, 2018. Trend of air quality in Seoul: policy and science. *Aerosol Air Qual. Res.* 18, 2141–2156. <https://doi.org/10.4209/aaqr.2018.03.0081>.
- Lamb, K.D., Perring, A.E., Samsel, B., Peterson, D., Davis, S., Anderson, B.E., et al., 2018. Estimating source region influences on black carbon abundance, microphysics, and radiative effect observed over South Korea. *J. Geophys. Res.: Atmospheres* 123, 548. <https://doi.org/10.1029/2018JD029257>, 13,527–13.
- Leahy, L.V., Anderson, T.L., Eck, T.F., Bergstrom, R.W., 2007. A synthesis of single scattering albedo of biomass burning aerosol over southern Africa during SAFARI 2000. *Geophys. Res. Lett.* 34, L12814. <https://doi.org/10.1029/2007GL029697>.
- Lee, J.Y., Kim, Y.P., 2007. Source apportionment of the particulate PAHs at Seoul, Korea: impact of long range transport to a megacity. *Atmos. Chem. Phys.* 7, 3587–3596. <https://doi.org/10.5194/acp-7-3587-2007>.
- Lee, S., Kim, J., Choi, M., Hong, J., Lim, H., Eck, T.F., Holben, B.N., Ahn, J.-Y., Kim, J., Koo, J.-H., 2019. Analysis of long-range transboundary transport (LRTT) effect on Korean aerosol pollution during the KORUS-AQ campaign. *Atmos. Environ.* 204, 53–67. <https://doi.org/10.1016/j.atmosenv.2019.02.020>. ISSN 1352-2310.
- Lennartson, E.M., Wang, J., Gu, J., Castro Garcia, L., Ge, C., Gao, M., Choi, M., Saide, P. E., Carmichael, G.R., Kim, J., Janz, S.J., 2018. Diurnal variation of aerosol optical depth and PM<sub>2.5</sub> in South Korea: a synthesis from AERONET, satellite (GOCI), KORUS-AQ observation, and the WRF-Chem model. *Atmos. Chem. Phys.* 18, 15125–15144. <https://doi.org/10.5194/acp-18-15125-2018>.
- Lelieveld, J., Evans, J.S., Fnais, M., Giannadaki, D., Pozzer, A., 2015. The contribution of outdoor air pollution sources to premature mortality on a global scale. *Nature* 525 (7569), 367–371. <https://doi.org/10.1038/nature15371>.
- Li, Z., Eck, T., Zhang, Y., Zhang, Y., Li, D., Li, L., Xu, H., Hou, W., Lv, Y., Goloub, P., Gu, X., 2014. Observations of residual submicron fine aerosol particles related to cloud and fog processing during a major pollution event in Beijing. *Atmos. Environ.* 86, 187–192. <https://doi.org/10.1016/j.atmosenv.2013.12.044>.
- Li, L., Hoffmann, M.R., Colussi, A.J., 2018. Role of nitrogen dioxide in the production of sulfate during Chinese haze-aerosol episodes. *Environ. Sci. Technol.* 52 (5), 2686–2693. <https://doi.org/10.1021/acs.est.7b05222>.
- Liu, Z., Fairlie, T.D., Uno, I., Huang, J., Wu, D., Omar, A., Kar, J., Vaughan, M., Rogers, R., Winker, D., Trepte, C., Hu, Y., Sun, W., Lin, B., Cheng, A., 2013.

- Transpacific transport and evolution of the optical properties of Asian dust. *J. Quant. Spectrosc. Radiat. Transf.* 116 (24), 33. <https://doi.org/10.1016/j.jqsrt.2012.11.011>. ISSN 0022-4073.
- Liu, Q., Cao, Ziqi, Qiu, Jingyi, Wang, Wencai, Zhou, Yang, Diao, Yina, Sheng, Lifang, 2018. Possible connection between the East Asian summer monsoon and a swing of the haze-fog-prone area in eastern. *China Theor. Appl. Climatol.* 132 (3–4), 1117–1127. <https://doi.org/10.1007/s00704-017-2137-2>.
- McNaughton, C.S., Clarke, A.D., Kapustin, V., Shinzuka, Y., Howell, S.G., Anderson, B. E., Winstead, E., Dibb, J., Scheuer, E., Cohen, R.C., Wooldridge, P., Perring, A., Huey, L.G., Kim, S., Jimenez, J.L., Dunlea, E.J., DeCarlo, P.F., Wennberg, P.O., Crounse, J.D., Weinheimer, A.J., Flocke, F., 2009. Observations of heterogeneous reactions between Asian pollution and mineral dust over the Eastern North Pacific during INTEX-B. *Atmos. Chem. Phys.* 9, 8283–8308. <https://doi.org/10.5194/acp-9-8283-2009>.
- Miao, Y., Guo, J., Liu, S., Liu, H., Zhang, G., Yan, Y., He, J., 2017. Relay transport of aerosols to Beijing-Tianjin-Hebei region by multi-scale atmospheric circulations. *Atmos. Environ.* 165, 35–45. <https://doi.org/10.1016/j.atmosenv.2017.06.032>. ISSN 1352-2310.
- Naimie, C.E., Blain, C.A., Lynch, D.R., 2001. Seasonal mean circulation in the Yellow Sea — a model-generated climatology. *Continent. Shelf Res.* 21 (6–7), 667–695. [https://doi.org/10.1016/S0278-4343\(00\)00102-3](https://doi.org/10.1016/S0278-4343(00)00102-3). ISSN 0278-4343.
- Nault, B.A., Campuzano-Jost, P., Day, D.A., Schroder, J.C., Anderson, B., Beyersdorf, A. J., Blake, D.R., Brune, W.H., Choi, Y., Corr, C.A., de Gouw, J.A., Dibb, J., DiGangi, J. P., Diskin, G.S., Fried, A., Huey, L.G., Kim, M.J., Knote, C.J., Lamb, K.D., Lee, T., Park, T., Pusede, S.E., Scheuer, E., Thornhill, K.L., Woo, J.-H., Jimenez, J.L., 2018. Secondary organic aerosol production from local emissions dominates the organic aerosol budget over Seoul, South Korea, during KORUS-AQ. *Atmos. Chem. Phys.* 18, 17769–17800. <https://doi.org/10.5194/acp-18-17769-2018>.
- O'Neill, N.T., Eck, T.F., Holben, B.N., Smirnov, A., Dubovik, O., Royer, A., 2001. Bimodal size distribution influences on the variation of Angstrom derivatives in spectral and optical depth space. *J. Geophys. Res.* 106, 9787–9806.
- O'Neill, N.T., Eck, T.F., Smirnov, A., Holben, B.N., Thulasiraman, S., 2003. Spectral discrimination of coarse and fine mode optical depth. *J. Geophys. Res.* 108 (D17), 4559. <https://doi.org/10.1029/2002JD002975>.
- Park, K.-A., Lee, E.-Y., Chang, E., Hong, S., 2015. Spatial and temporal variability of sea surface temperature and warming trends in the Yellow Sea. *J. Mar. Syst.* 143 (24), 38. <https://doi.org/10.1016/j.jmarsys.2014.10.013>. ISSN 0924-7963.
- Park, S., Shin, M., Im, J., Song, C.-K., Choi, M., Kim, J., Lee, S., Park, R., Kim, J., Lee, D.-W., Kim, S.-K., 2019. Estimation of ground-level particulate matter concentrations through the synergistic use of satellite observations and process-based models over South Korea. *Atmos. Chem. Phys.* 19, 1097–1113. <https://doi.org/10.5194/acp-19-1097-2019>.
- Peterson, D.A., Hyer, E.J., Han, S.-O., Crawford, J.H., Park, R., Holz, R., Kuehn, R.E., Eloranta, E., Lefer, B.L., 2019. Meteorology Influencing Springtime Air Quality and Pollution Transport in Korea. *Elem. Sci. Anth.* <https://doi.org/10.1525/elementa.395>.
- Pueschel, R.F., Russell, P.B., Allen, D.A., Ferry, G.V., Snetsinger, K.G., Livingston, J.M., Verma, S., 1994. Physical and optical properties of the Pinatubo volcanic aerosol: aircraft observations with impactors and a Sun-tracking photometer. *J. Geophys. Res.* 99 (D6), 12,915–12,922.
- Reid, J.S., Eck, T.F., Christopher, S.A., Hobbs, P.V., Holben, B.R., 1999. Use of the Angstrom exponent to estimate the variability of optical and physical properties of aging smoke particles in Brazil. *J. Geophys. Res.* 104 (27), 489–27,489.
- Reid, J.S., Eck, T.F., Christopher, S.A., Koppmann, R., Dubovik, O., Eleuterio, D.P., Holben, B.N., Reid, E.A., Zhang, J., 2005. A review of biomass burning emissions part III: intensive optical properties of biomass burning particles. *Atmos. Chem. Phys.* 5, 827–849.
- Reid, J.S., Brooks, B., Crahan, K.K., Hegg, D.A., Eck, T.F., O'Neill, N., de Leeuw, G., Reid, E.A., Anderson, K.D., 2006. Reconciliation of coarse mode sea-salt aerosol particle size measurements and parameterizations at a subtropical ocean receptor site. *J. Geophys. Res.* 111, D02202. <https://doi.org/10.1029/2005JD006200>.
- Reid, J.S., Reid, E.A., Walker, A., Piketh, S., Cliff, S., Al Mandoos, A., Tsay, S.-C., Eck, T. F., 2008. Dynamics of southwest Asian dust particle size characteristics with implications for global dust research. *J. Geophys. Res.* 113, D14212. <https://doi.org/10.1029/2007JD009752>.
- Reid, J.S., et al., 2017. Ground-based High Spectral Resolution Lidar observation of aerosol vertical distribution in the summertime Southeast United States. *J. Geophys. Res. Atmos.* 122, 2970–3004. <https://doi.org/10.1002/2016JD025798>.
- Schafer, J.S., Eck, T.F., Holben, B.N., Thornhill, K.L., Anderson, B.E., Sinyuk, A., Giles, D. M., Winstead, E.L., Ziemba, L.D., Beyersdorf, A.J., Kenny, P.R., Smirnov, A., Slutsker, I., 2014. Intercomparison of aerosol single scattering albedo derived from AERONET surface radiometers and LARGe in situ aircraft profiles during the 2011 DRAGON-MD and DISCOVER-AQ experiments. *J. Geophys. Res. Atmos.* 119 (12), 7439–7452. <https://doi.org/10.1002/2013JD021166>. JUN 27 2014.
- Schafer, J.S., Eck, T.F., Holben, B.N., Thornhill, K.L., Ziemba, L.D., Sawamura, P., Moore, R.H., Slutsker, I., Anderson, B.E., Sinyuk, A., Giles, D.M., Smirnov, A., Beyersdorf, A.J., Winstead, E.L., 2019. Intercomparison of aerosol volume size distributions derived from AERONET ground-based remote sensing and LARGe in situ aircraft profiles during the 2011–2014 DRAGON and DISCOVER-AQ experiments. *Atmos. Meas. Technol.* 12, 5289–5301. <https://doi.org/10.5194/amt-12-5289-2019>.
- Schmid, B., Michalsky, J., Halthore, R., Beauharnois, M., Harrison, L., Livingston, J., Russell, P., Holben, B., Eck, T., Smirnov, A., 1999. Comparison of aerosol optical depth from four solar radiometers during the fall 1997 ARM intensive observation period. *Geophys. Res. Lett.* 26, 2725–2728.
- Shi, G., Xu, J., Shi, X., Liu, B., Bi, X., Xiao, Z., et al., 2019. Aerosol pH dynamics during intense haze periods in an urban environment in China: use of detailed, hourly, speciated observations to study the role of ammonia availability and secondary aerosol formation and urban environment. *J. Geophys. Res.: Atmospheres* 124. <https://doi.org/10.1029/2018JD029976>.
- Sinyuk, A., Holben, B.N., Eck, T.F., Giles, D.M., Slutsker, I., Korkin, S., Schafer, J.S., Smirnov, A., Sorokin, M., Lyapustin, A., 2020. The AERONET Version 3 aerosol retrieval algorithm, associated uncertainties and comparisons to Version 2. *Atmos. Chem. Phys. Discuss.*
- Smirnov, A., Holben, B.N., Dubovik, O., Frouin, R., Eck, T.F., Slutsker, I., 2003. Maritime component in aerosol optical models derived from Aerosol Robotic Network data. *J. Geophys. Res.* 108 (D1), 4033. <https://doi.org/10.1029/2002JD002701>.
- Thompson, A.M., Stauffer, R.M., Boyle, T.P., Kollonige, D.E., Miyazaki, K., Tzortziou, M., et al., 2019. Comparison of near-surface NO<sub>2</sub> pollution with pandora total column NO<sub>2</sub> during the Korea-United States ocean color (KORUS OC) campaign. *J. Geophys. Res.: Atmospheres* 124. <https://doi.org/10.1029/2019JD030765>.
- Toth, T.D., Zhang, J., Campbell, J.R., Hyer, E.J., Reid, J.S., Shi, Y., Westphal, D.L., 2014. Impact of data quality and surface-to-column representativeness on the PM<sub>2.5</sub>/satellite AOD relationship for the contiguous United States. *Atmos. Chem. Phys.* 14, 6049–6062. <https://doi.org/10.5194/acp-14-6049-2014>.
- van Donkelaar, A., Martin, R.V., Brauer, M., Kahn, R., Levy, R., Verduzco, C., Villeneuve, P.J., 2010. Global estimates of ambient fine particulate matter concentrations from satellite-based aerosol optical depth: development and application. *Environ. Health Perspect.* 118, 6. <https://doi.org/10.1289/ehp.0901623>.
- Virkkula, A., 2010. Correction of the calibration of the 3-wavelength particle soot absorption photometer (3λ PSAP). *Aerosol. Sci. Technol.* 44 (8), 706–712. <https://doi.org/10.1080/02786826.2010.482110>.
- Wang, Y., Wang, M., Zhang, R., Ghan, S.J., Lin, Y., Hu, J., Pan, B., Levy, M., Jiang, J.H., Molina, M.J., 2014. Assessing the effects of anthropogenic aerosols on Pacific storm track using a multiscale global climate model. *Proc. Natl. Acad. Sci. Unit. States Am.* 201403364. <https://doi.org/10.1073/pnas.1403364111>.
- Wang, W., Zhang, R., Gomez, M.E., Yang, L., Zamora, M.L., Hu, M., Lin, Y., Peng, J., Guo, S., Meng, J., Li, J., Cheng, C., Hu, T., Ren, Y., Wang, Y., Gao, J., Cao, J., An, Z., Zhou, W., Li, G., Wang, J., Tian, P., MarreroOrtiz, W., Secret, J., Du, Z., Zheng, J., Shang, D., Zeng, L., Shao, M., Wang, W., Huang, Y., Wang, Y., jZhu, Y., Li, Y., Hu, J., Pan, B., Cai, L., Cheng, Y., Ji, Y., Zhang, F., Rosenfeld, D., Liss, P.S., Duce, R.A., Kolb, C.E., Molina, M.J., 2016. Persistent sulfate formation from London Fog to Chinese haze. *Proc. Natl. Acad. Sci.* 113 (48), 13630–13635. <https://doi.org/10.1073/pnas.1616540113>, 2016.
- Wu, J., Bei, N., Hu, B., Liu, S., Zhou, M., Wang, Q., Li, X., Liu, L., Feng, T., Liu, Z., Wang, Y., Cao, J., Tie, X., Wang, J., Molina, L.T., Li, G., 2019. Is water vapor a key player of the wintertime haze in North China Plain? *Atmos. Chem. Phys.* 19, 8721–8739. <https://doi.org/10.5194/acp-19-8721-2019>.
- Yoshitomi, M., Wild, O., Akimoto, H., 2011. Contributions of regional and intercontinental transport to surface ozone in the Tokyo area. *Atmos. Chem. Phys.* 11, 7583–7599. <https://doi.org/10.5194/acp-11-7583-2011>.
- Zhang, R., Li, G., Fan, J., Wu, D.L., Molina, M.J., 2007. Intensification of Pacific storm track linked to Asian pollution. *Proc. Natl. Acad. Sci. Unit. States Am.* 104 (13), 5295–5299. <https://doi.org/10.1073/pnas.0700618104>.
- Zhang, J., Reid, J.S., 2009. An analysis of clear sky and contextual biases using an operational over ocean MODIS aerosol product. *Geophys. Res. Lett.* 36, L15824. <https://doi.org/10.1029/2009GL038723>.
- Zhong, J., Zhang, X., Wang, Y., Sun, J., Zhang, Y., Wang, J., Tan, K., Shen, X., Che, H., Zhang, L., Zhang, Z., Qi, X., Zhao, H., Ren, S., Li, Y., 2017. Relative contributions of boundary-layer meteorological factors to the explosive growth of PM<sub>2.5</sub> during the red-alert heavy pollution episodes in Beijing in December 2016. *J. Meteorol. Res.* 31, 809. <https://doi.org/10.1007/s13351-017-7088-0>.
- Zhong, J., Zhang, X., Dong, Y., Wang, Y., Liu, C., Wang, J., Zhang, Y., Che, H., 2018. Feedback effects of boundary-layer meteorological factors on cumulative explosive growth of PM<sub>2.5</sub> during winter heavy pollution episodes in Beijing from 2013 to 2016. *Atmos. Chem. Phys.* 18, 247–258. <https://doi.org/10.5194/acp-18-247-2018>.
- Ziemba, L.D., et al., 2013. Airborne observations of aerosol extinction by in situ and remote-sensing techniques: evaluation of particle hygroscopicity. *Geophys. Res. Lett.* 40, 417–422. <https://doi.org/10.1029/2012GL054428>.